EUROPEAN ORGANIZATION FOR NUCLEAR RESEARCH

CERN - PPE / 95-183

CMS TN / 95 - 167

November 16th 1995

THE CMS DETECTOR AND PHYSICS AT THE LHC

D. Denegri,

CERN / PPE

For the CMS Collaboration

ABSTRACT

We discuss the physics issues at the LHC, the CMS detector, one of the two general purpose detectors planned at the LHC, and the expected physics performance of LHC detectors in the search for SM and SUSY Higgs bosons, some SUSY particle searches and some possibilities in B and heavy ion physics.

Invited talk given at the

Conference on Elementary Particle Physics, Present and Future

Valencia, Spain, June 1995

THE CMS DETECTOR AND PHYSICS AT THE LHC

D. Denegri, CERN / PPE
For the CMS Collaboration

1. INTRODUCTION

The main motivation for building the LHC is to investigate the mechanism responsible for electroweak symmetry breaking. The Standard Model (SM) Higgs mechanism is such a possibility [1]. The Minimal Supersymmetric Standard Model (MSSM) is a possible extention, but alternative symmetry breaking schemes with strongly interacting W_L, Z_L in the TeV mass range have been proposed too [2]. The present mass constraints on the SM Higgs are loose ($m_H < 1$ TeV) [1]. The design and optimisation of an LHC detector to be able to explore the entire expected SM Higgs mass range taking into account the the variety of decay modes and expected experimental signatures is an adequate design criterion. It provides enough flexibility to allow an investigation of the ew symmetry breaking mechanism, even if there were no elementary Higgs bosons. The ATLAS and CMS collaborations propose to build detectors designed for such investigations at the highest luminosities available ($L \approx 10^{34}$ cm^{-2}s^{-1}) in $\sqrt{s} = 14$ TeV proton–proton collisions at the LHC.

The CMS detector (Fig.1) is built around a large, 13m long, 6m diameter, high-field superconducting solenoid (4 T) leading to a compact design for the muon spectrometer, hence the name Compact Muon Solenoid (CMS) [3]. The hadronic and electromagnetic calorimeters are located inside the coil. The innermost part of the detector is occupied by a 6m long, 1.3m radius central tracker. To detect signatures of new physics efficiently, identification and precise measurement of muons, photons and electrons is emphasised in the design of CMS. The goal of this experiment is to measure these particles with an energy resolution of about 1% over a large momentum range.

The central feature of the ATLAS detector (Fig.2) is a large air-core toroidal magnet muon spectrometer consisting of an 8-coils barrel toroid with 0.8 T average field, each coil being 26m long and 4.7m wide, and two endcap toroids [4]. This system would allow precise muon measurements at highest luminosities using the external muon system alone. The measurements are done in the air behind calorimeters that have absorbed all the hadrons. The electromagnetic calorimeter is a liquid argon one with a particular "accordion" geometry. A thin 2T solenoid is placed in front of the em calorimeter to allow momentum measurements in the inner tracker of similar dimension to the CMS one. Although the goals of these two general purpose detectors are very much the same, the experimental techniques are different and complementary, in particular in the B-field configuration and calorimeter choices.

With the investigation of the origine of particle masses, the second, and not unrelated, most important task for these detectors will be the search for the supersymmetric partners of Standard Model particles. The production cross sections for the strongly interacting squarks and gluinos are large at hadron colliders. At the LHC this allows to search for these particles up to a mass of ~ 2TeV ie over the range where supersymmetry could be relevant to ew symmetry breaking. A significant discovery potential also exists for sleptons and charginos / neutralinos for masses up to ~ 0.2 TeV [5]. Particularly important would be the (indirect) detection of the lightest neutralino as the LSP as it is the best cold (or mixed) dark matter candidate. Introduction of supersymmetry cures the mass divergence problems of the SM Higgs, but at the expense of introducing several Higgs bosons [6]. In the MSSM there are five such states and they can be investigated over a large portion of parameter space in ATLAS and CMS. Detector requirements for the search for the MSSM Higgs bosons are similar as for the SM Higgs. Searches for squarks and gluinos depend crucially on the missing momentum measurements. Both detectors are thus designed to be highly hermetic. Missing momentum resolution is important in detecting MSSM Higgs modes with τ's in the final state, $H^{\pm} \rightarrow \tau\nu$ and h, H, A $\rightarrow \tau\tau$.

Although high luminosity is essential to cover the entire range of mechanisms of electroweak symmetry breaking and explore a significant fraction of SUSY parameter space, the LHC will start at a significantly lower luminosity. Both the ATLAS and CMS detectors are designed to take full benefit of the lower luminosities ($L \leq 10^{33}$ $cm^{-2}s^{-1}$) to study large cross-section phenomena such as beauty and top production. Such studies require powerful inner tracking and microvertexing systems. The recent observation by CDF of a number of exclusive modes $B \rightarrow J/\psi K_s^0$, $J/\psi K^{\pm}$, $J/\psi K^*$, $J/\psi\phi$ shows that at least some exclusive B channels can be extracted with a good signal to noise ratio[7]. The 10^{12} to 10^{13} $b\bar{b}$ produced per year at the LHC should allow the study of CP violation in the B sector, and of some rare B decays, such as $B \rightarrow \mu\mu$, testing physics beyond the Standard Model. B-factories at $10^{33}cm^{-2}s^{-1}$ are limited to few times 10^7 $b\bar{b}$/year, whilst CDF/D0 or HERA/B to ~10^9 $b\bar{b}$/year. A dedicated B-physics detector, LHC-B, is also under active study [8]. It would be a single arm spectrometer covering the angular range from ~ 10 mrad to ~ 400 mrad to the beam line, optimised for data the 10^{32} to ~10^{33} $cm^{-2}s^{-1}$ range.

An important part of the LHC physics programme will be devoted to heavy ion collisions. The expected luminosities go from $10^{27}cm^{-2}s^{-1}$ in Pb-Pb collisions to $3x10^{31}cm^{-2}s^{-1}$ in O-O collisions. The nucleon-nucleon center of mass energy would be 5.4 TeV. Heavy ion beams at LHC should provide collision energy densities well above the expected threshold for formation of a quark-gluon plasma. A dedicated detector, ALICE [9], is being considered for studies of a broad range of signatures of quark-gluon plasma formation. The emphasis in this detector is on efficient detection of soft particles and on particle identification; a limited solid angle calorimetric coverage is foreseen and a possibility to adjoin a muon spectrometer is also contemplated. Particular signatures of quark-gluon plasma could be looked for in the general purpose detectors too. Colour screening effects on heavy quark bound states is such a possibility [10]. The CMS collaboration plans to measure the $\mu^+\mu^-$ rates in the Υ family and study the suppression of $\Upsilon(2S)$ and $\Upsilon(3S)$ relative to $\Upsilon(1S)$ with different ion species, and relative to pp collisions [3]. The muon arm in ALICE could allow to perform these studies too.

In the following we discuss in more detail the CMS detector as an example of a general purpose detector at LHC, then we discuss the expected physics performance and reach for SM and SUSY Higgs boson searches, make some remarks on SUSY particle searches and finally we give some examples of B and heavy ion physics possibilities at the LHC.

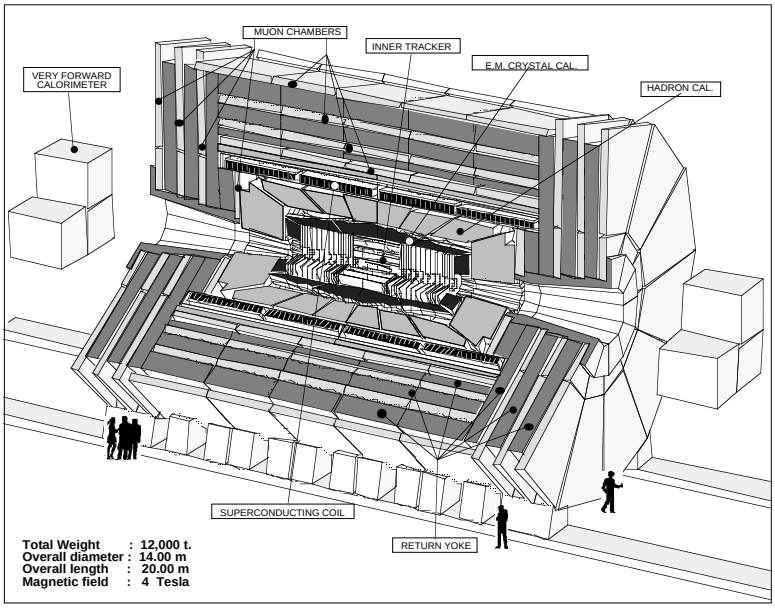

Fig. 1 : Three-dimensional view of CMS

Fig. 2 Three-dimensional view of the ATLAS detector. The overall length is 40m and the diameter 20m.

2. THE CMS DETECTOR

Magnet

The central piece of CMS is a long solenoid (L = 13m) with an inner radius of 2.95 m generating a uniform magnetic field of 4 T [1]. The magnetic flux is returned through a 1.8 m thick saturated iron yoke (1.8 T) instrumented with muon chambers. The integral bending power of the solenoid is 17 Tm up to rapidity of 1.5 and decreases to ≈ 6 Tm at $|\eta| = 2.5$. A single magnet thus provides the necessary bending power for precise inner and muon tracking, and efficient muon detection and measurement up to rapidities of 2.5. Measurements within the iron yoke provide the muon stand-alone capability. Figure 1 shows a 3-dimensional view of CMS. The overall dimensions of the detector are: a length of about 22 m, a diameter of 14.6 m and a total weight of 14500 tons .

Muon system

The 4 T solenoidal field leads to an excellent momentum resolution and facilitates sharp muon momentum thresholds at trigger level. Starting from the primary vertex, muons are first measured in the inner tracker, then traverse the calorimeters, the coil and a return yoke (Fig. 3). They are identified and measured in four muon stations inserted in the return yoke in the barrel and endcap regions. The four stations provide redundancy and optimize geometrical acceptance. The four muon stations also include triggering planes that identify the bunch crossing and enable a cut on the muon transverse momentum at the first trigger level. This arrangement of chambers (Fig. 3) allows low p_t (~ 4 GeV) muon triggers required for CP violation studies and for the study of $\Upsilon(\Upsilon',\Upsilon'') \rightarrow \mu^+\mu^-$ production in heavy ion collisions.

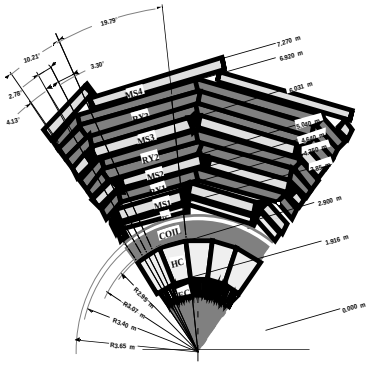

Fig. 3: Transverse view of CMS in the barrel region with the four muon stations MS1 to MS4 .

In a barrel muon station, about 40 cm deep, two groups of 4 layers of aluminium DTBX chambers (drift tubes with bunch crossing capability) are used in the bending plane to measure precisely the $r\phi$ coordinate and the local trajectory slope, and to define the bunch crossing using a mean-timer technique [11]. They are supplemented by 4 DTBX layers for the measurement of the other (z) coordinate. There are about 2×10^5 drift tube channels in the barrel. The goal is to achieve a space resolution of better than ≈200 μm per layer giving a position accuracy of ≈ 100 μm and angular accuracy of ≈ 1mrad per station. At trigger level the DTBX system provides a local trajectory slope with ~ 15 mrad accuracy. A time resolution of much better than 25ns is needed to identify the bunch crossing. Six layers of resistive plate chambers (RPC), two in MS1 and MS2 and one in MS3 and MS4, with an excellent time resolution (σ ~2nsec) and sufficient spatial resolution are also used in a first-level muon trigger [12]. The four endcap muon stations which must work in a magnetic field use six-layer CSC (cathode strip chambers) for precision measurement of muon position and momentum [13]. The precision of CSC's is ~ 100μm per layer. The CSC's are also used for triggering and they are supplemented, as the DTBX's in the barrel region, by the RPC trigger system which extends up to $|\eta| = 2.1$. This double triggering scheme insures robustness of muon triggering.

In CMS the lowest values of the muon thresholds (determined by muon penetration through calorimeters) for 90% trigger efficiency in various rapidity ranges are the following:

$p_t^{\mu} >$ 4.3 GeV for: 0.0< $|\eta| \leq$1.5:

$p_t^{\mu} >$ 3.4 GeV for: 1.5< $|\eta| \leq$2.0:

$p_t^{\mu} >$ 2.4 GeV for: 2.0< $|\eta| \leq$2.5:

These thresholds will be useful for multi-muon final states at ~$10^{33}cm^{-2}s^{-1}$, in B physics studies or in heavy ion runs in particular. Two-muon final states from Z or Higgs decays are less demanding, requiring p_t^{μ} > 7-10 GeV. At $10^{34}cm^{-2}s^{-1}$ the di-muon trigger would have a threshold at ~10 GeV and the more demanding, rate limited, single muon trigger with a threshold at 20 GeV would result in a 6kHz first-level trigger output rate [3]. If the magnetic field were reduced to 3T the same trigger threshold would lead to a 10 kHz first-level trigger rate.

Tracking

The goal of the inner tracking system of CMS is to reconstruct high p_t muons and isolated electrons in $|\eta| < 2.5$ with a momentum resolution of $\Delta p_T / p_T \approx 0.15 p_T \oplus 0.5\%$ (p_T in TeV), as well as hadrons down to low transverse momenta ($\geq$ 2 GeV). Lepton and photon isolation is a very important criterion in signal selection for a number of important signals such as $H_{SM,\ susy} \rightarrow ZZ^* \rightarrow 2\ l^+2l^-$, $H_{SM,SUSY} \rightarrow \gamma\gamma$ or in sparticle searches, in particular for sleptons, charginos, neutralinos leading to leptons in the final state [5,3]. To identify isolated leptons or photons it is thus important to reconstruct all high p_T tracks (p_T > 2 GeV) including hadrons in the central rapidity region. Track measurement, counting and isolation is also the main requirement in selecting τ candidates. An excellent momentum resolution (≤1 % below 100 GeV) is needed for electromagnetic calorimeter calibration through E/p matching using $Z \rightarrow e^+e^-$ and $W \rightarrow e\nu$ decays, and is desirable for a good signal to background ratio for narrow states such as $J/\Psi \rightarrow \mu^+\mu^-$, $\Upsilon(\Upsilon',\Upsilon'') \rightarrow \mu^+\mu^-$, $B_d^0 \rightarrow \pi^+\pi^-$, $B_s^0 \rightarrow \mu^+\mu^-$ or $Z \rightarrow l^+l^-$, $H_{SM} \rightarrow ZZ^* \rightarrow 2\ l^+2l^-$, $H_{SUSY} \rightarrow ZZ^*$, $ZZ \rightarrow 2\ l^+2l$, and h, H, A $\rightarrow \mu^+\mu^-$.

The main problem in tracking is that of pattern recognition. At a luminosity of $10^{34}cm^{-2}s^{-1}$, interesting events will be superimposed on a background of about 500 soft charged tracks within the rapidity range considered from ~15 minimum bias events occurring in the same bunch crossing. Their vertices are distributed along the beam direction (z-axis) with a r.m.s. of 5.3 cm. To solve the pattern recognition problem at high luminosity detectors with small cell sizes are required. In CMS silicon and gas microstrip detectors provide the required granularity and precision. Strip lengths of the order of 10 cm are necessary to maintain the cell occupancies below 1%. This leads to a large number of detection channels ($\approx 10^7$).

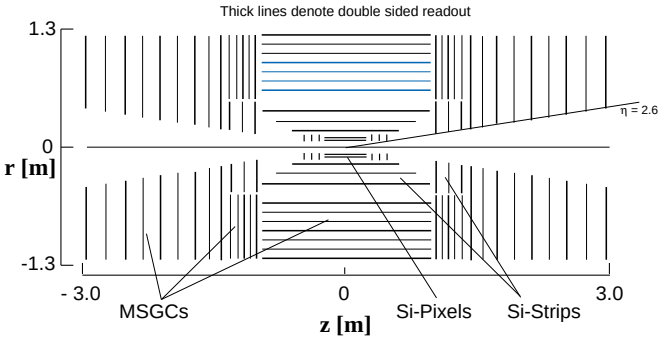

Fig. 4: Layout of the CMS Tracker

Figure 4 shows how the detector planes are distributed in the cylindrical tracking volume of CMS with dimensions $|z| < 3.0$ m, $R < 1.2$ m. The detailed design of the tracker is still evolving. A track in the barrel part of the tracker encounters first two layers of pixel detectors (125 x 125μm^2) providing a measurement accuracy of 15 μm, then three layers of microstrip Si detectors of 50 μm pitch, 125mm long providing high precision points of 15 μm accuracy, followed by seven layers of 200 μm pitch, 125 or 250 mm long gas microstrip chambers (MSGC) giving a measurement with ≈50 μm precision at normal incidence[14]. The forward tracking system is made of detector elements mounted in concentric rings on disks with silicon strip detectors and MSGC detectors. The total number of channels is $11x10^6$ for MSCG's and $3x10^6$ for silicon detectors. High track

finding efficiencies are expected for isolated tracks, as well as for tracks in jets, the mean efficiency in $|\eta| < 2.5$ is about 95% even inside jets [3, 15]. Figure 5 shows the expected track momentum resolutions in the CMS tracker alone. For high momentum muons the combination of tracker and muon chamber measurements improves very much the resolution: $\Delta p_T / p_T \approx 0.06$ for a p =1 TeV muon in $|\eta| < 1.6$ [3]. The relative alignement precision required for the inner tracker and external muon system is ~ 100 μm.

The two pixel layers at a radial distance of 7.5 and 11 cm from the beam line (Fig. 4) with the three forward pixel discs, altogether 80×10^6 channels, insure precise impact parameter measurements, with an asymptotic (high momentum) accuracy of σ_{IP} = 23 μm in the transverse plane, Fig. 5 [3]. The possibility to bring the inner layer to a ~4cm radius for initial low luminosity running is also being considered. Impact parameter measurements play an essential role in B-physics (CP violation, B^0 oscillations) and in tagging b-jets in high p_t events, such as $t\bar{t}$ production, associated $b\bar{b}H$ production, in the search for $H \rightarrow b\bar{b}$ decays, as well as for modes involving τ's ($H^{\pm} \rightarrow \tau\nu$ and h, H, A $\rightarrow \tau\tau$). Microvertex b-tagging played a key role in the recent discovery of top. The pixels are also very useful for pattern recognition.

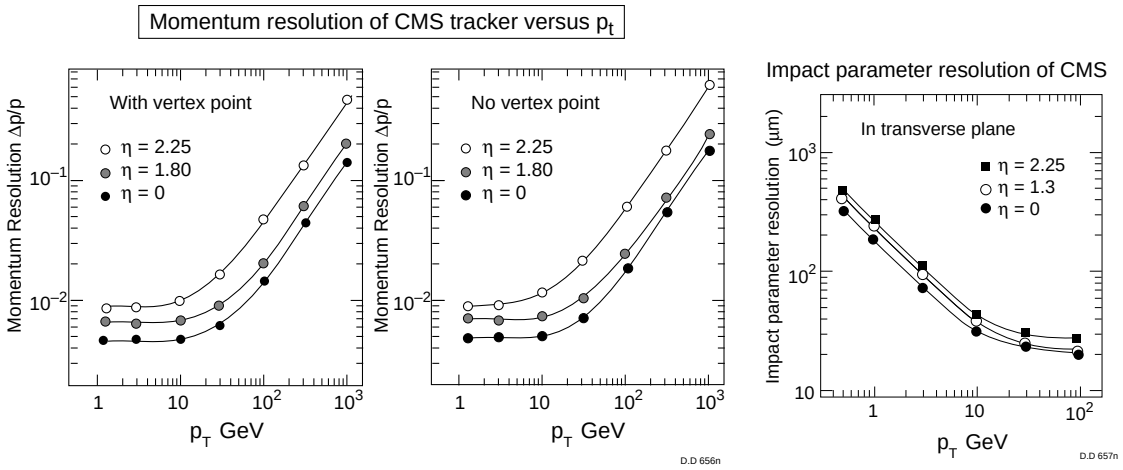

Fig. 5: Momentum and impact parameter resolutions as a function of p_t at various rapidities.

Calorimetry

The primary function of the electromagnetic (EM) calorimeter is to measure precisely electrons and photons. In conjunction with the hadron calorimeter it measures also jets. The calorimeter system of CMS, is made of a high resolution lead-tungstate ($PbWO_4$) crystal EM calorimeter and the hadron calorimeter behind it. In the endcap region the EM calorimetry extends up to rapidity 2.6 (possibly up to 3.0) and the hadron calorimeter up to $|\eta| = 3.0$. This central calorimetric system is complemented in the forward region $3.0 < |\eta| < 5.0$ by 'very forward calorimeters' (Fig.1). Their function is to insure detector hermeticity for good missing transverse energy resolution, and to measure forward 'tagging' jets signing Higgs production through WW or ZZ fusion. Hermeticity is particularly important for processes where the physical missing E_t is on the order of few tens of GeV as in h, H, A $\rightarrow \tau\tau$, W $\rightarrow l\nu$, t $\rightarrow l\nu$ b, t $\rightarrow H^{\pm}b \rightarrow \tau\nu$ b and for sparticle searches connecting the LEP2 and Fermilab with the LHC search ranges.

The desired performance, choice of detection technique and design of the EM calorimeter is to a large extent determined by the requirements imposed by the $H \rightarrow \gamma\gamma$ channel. This is the most appropriate channel to search at a hadron collider the SM Higgs boson or the lightest MSSM Higgs boson h in the ≈ 80 - 130 GeV mass range. The natural width of the Higgs in this mass range is very small (<<1 GeV) thus the observed signal width is entirely determined by the experimental γγ effective mass resolution. This resolution and the level of the large and irreducible γγ background ultimately determine the signal significance. To achieve a high mass resolution requires first an excellent electromagnetic energy resolution σ_E / E. However the γγ mass resolution depends also on the two-photon angular separation θ:

$$\sigma_M / M = 1/2(\sigma_{E1}/E_1 \oplus \sigma_{E2}/E_2 \oplus \sigma_\theta/tg\theta/2) \qquad (\oplus \text{ are quadratic sums})$$

At ~10^{33} cm^{-2}s^{-1} the event vertex is known or is effectively designated by a hard track in the event [16] and the angular term has only a minor effect on the $\gamma\gamma$ mass resolution (a contribution $\delta m_{\gamma\gamma} < 200$ MeV). At 10^{34} cm^{-2}s^{-1} there are, however, on average 15 minimum bias events superimposed on the triggered $\gamma\gamma$ event. If the mean longitudinal vertex position were used in calculating the $\gamma\gamma$ effective mass, too large a contribution to the measured signal width would be introduced [17]. It is thus necessary to foresee a photon direction measurement capability for full luminosity running (would be needed at > 6x10^{33} cm^{-2}s^{-1}[16]). A directional precision of $\approx$ 8mrads is sufficient to keep this contribution to the resolution to < 500 MeV. This can be obtained from the shower position measurements in the calorimeter and a preshower detector located in front, Fig. 6 [3]. The goal is to have an overall resolution $\sigma_M \approx 800$ MeV for $m_H = 100$ GeV at 10^{34} cm^{-2}s^{-1}.

CMS has chosen a $PbWO_4$ crystal calorimeter. The main reasons for choosing this crystal are its short radiation length (9mm) and small Moliere radius (2.0cm) leading to a compact calorimeter, the short scintillation decay time constant matched to the 25 nsec bunch spacing, and good radiation hardness (with Nb doping) [18]. The low light-yield of this crystal can be overcome using Si avalanche photodiodes (or more radiation hard phototetrodes in the end-caps) as readout elements [19]. The arrangement of crystals is shown in Fig. 6. In the barrel the crystals have a length of 23 cm(25X_0 deep) and the lateral granularity is $\approx$ 2cm x 2cm (front face) i.e. $\Delta\eta$ x $\Delta\phi$ = 0.014 x 0.014. The preshower, 3X_0 deep, would cover in the barrel $|\eta| < 1.1$. The total volume of crystals is about 11 m^3 and the total number of crystals (channels) is $\approx 1.1\times10^5$. With such a calorimeter an energy resolution of $\sigma_E/E \approx 0.6\%$ can be expected for electrons (photons) of E_t = 120 GeV. This is at present obtained (0.7%) with prototypes in a test beam [20]. Calibrating and monitoring the response of the calorimeter at the required level is a major task and requires in-situ calibration. This is possible with E/p matching using the better than 1% precision momentum measurements of isolated electrons from W and Z decays [3, 21].

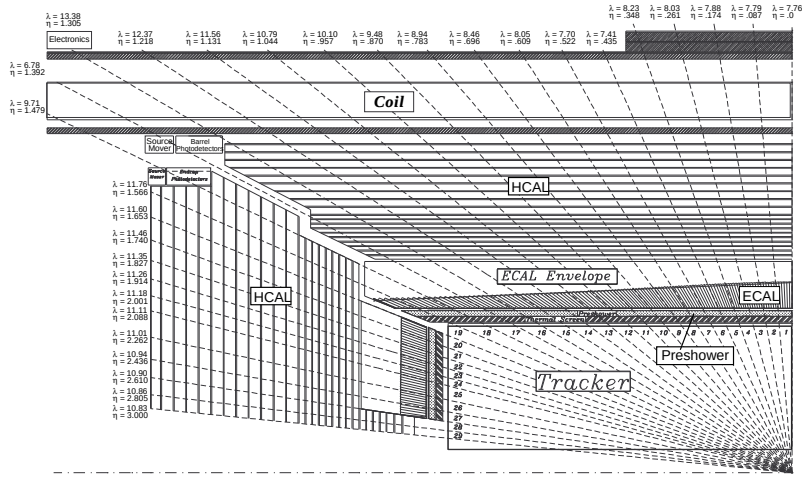

Fig. 6: Layout of the electromagnetic calorimeter, preshower and hadron calorimeter of CMS. The tower structure of the hadron calorimeter is indicated.

Hadron calorimetry with large geometrical coverage for measurement of multi-jet final states and missing transverse energy is essential in both squark and gluino searches, and for detection of the Higgs at m_H > 700 GeV. Hadron calorimetry plays also an essential role in t-quark physics, QCD jet studies and in channels involving τ's in the final state.

In CMS the hadron calorimeter is made of copper absorber plates interleaved with scintillator tiles read-out with embedded wavelength shifting fibers. The expected hadronic resolution is $\sigma_E/E = 70\%/\sqrt{E} \oplus 5\%$. The tiles are organised in towers (Fig. 6) giving a lateral segmentation of $\Delta\eta$ x $\Delta\phi \approx 0.09$ x 0.09, adequate for good di-

jet separation and mass resolution. Particularly demanding in this respect is the reconstruction of highly boosted W or Z decaying to two jets, produced in decays of a ~ 1 TeV mass Higgs. The main concern for the very forward calorimeters are the very high radiation levels expected in the region $3.0 < |\eta| < 5.0$. The two techniques considered at present are a sampling calorimeter with Fe plates and PPC's (parallel plate chambers)[22], or a quartz-fiber calorimeter [23].

Trigger and data acquisition

The task of the trigger system is to reduce the input rate of $\sim 10^9$ events/sec at high luminosity to <100Hz, the maximum rate at which events can be written on the permanent storage device. The average event size is ~ 1MByte, most of the information being provided by the tracker. The needed data reduction is done in two steps. The level-1 trigger system, using only calorimetric and muon system information in hardware processors operating at 40MHz input rate reduces the data rate to < 100kHz. To remain well within this cumulative first-level trigger output rate at 10^{34} $cm^{-2}s^{-1}$, typical trigger thresholds would be: for single electron (γ) $E_t > 30$ GeV, di-electrons (γ's) $E_t > 15$ GeV on each, for inclusive jets $E_t > 140$ GeV, for single muons $p_t > 20$ GeV, for dimuons $p_t > 10$ GeV, all within $|\eta| < 2.5$, and $E_t^{miss} > 150$ GeV [3].

For the higher-level triggers, a high bandwidth (≈ 500 Gbit/s) readout network (event builder) treating the ≈ 1000 front-end readout units with ~ 1000 Bytes/event and a high processing power (10^6-10^7 MIPS) event filter is needed [3]. The event filter is implemented in an on-line processor farm (about 1000 units) where full detector analysis and event reconstruction is performed, reducing the event rate by a factor ~ 1000 for writing on mass storage. The total data production will be on the order of 1TByte/day.

Collaborations, costs and schedule

At present all subdetectors in CMS have been chosen, except for the very-forward calorimeters. The evaluation of the cost of the major components of the detector is the following: the coil 74 MSF, the tracker 90 MSF, the EM calorimeter 80 MSF, the hadron calorimeter 42 MSF, the muon system 63 MSF, the trigger/DAQ system 47MSF and the iron yoke about 42 MSF. The overall cost of the CMS detector is estimated at 475 MSF [3]. The cost of the ATLAS detector is comparable [4].

The two collaborations ATLAS and CMS are also of comparable size, with at present about 1350 physicists and engineers from about 130 institutions in about 30 countries in each of them. About 50% of collaborators in CMS and about 40% in ATLAS are from CERN non-member states. The number of physicists from the US approaches 300 in each collaboration, with a somewhat smaller but comparable number from Russia and other Dubna-member states [3,4]. At present the number of physiciste and engineers in ALICE is about 300 and the cost of the detector is of the order of 120 MSF, whilst for LHCB it is ~150 participants and ~ 85 MSF.

With the LHC approved in December 1994 and a possible first-stage approval of CMS and ATLAS by the end of 1995, taking into account prototype construction and testing, detector construction, assembly and tests, civil engineering and installation, these detectors could be completed in 2004 [3,4].

3. PHYSICS AT THE LHC

Extensive studies have been made of the expected performance of CMS and ATLAS [3.4]. We discuss expectations for the SM Higgs boson and some of the MSSM Higgs bosons, and comment on the gluino and squark mass reaches, some CP-violation measurements and possible signals for QCD deconfinement via the relative suppressions within the *Y* family.

Signals have been evaluated for $\sqrt{s} = 14$TeV using in most cases PYTHIA, ISAJET is used for SUSY signals. For channels that are particularly sensitive rather complete GEANT simulations of detector responses are performed, but often GEANT simulations of momentum resolution, radiative losses, isolation efficiencies have been parameterised and implemented with Gaussian smearings [3,4].

3.1 Standard Model Higgs Boson

Fits of radiative corrections to electroweak data provide indirect information on m_H. The dependence is quadratic on m_{top}, but is only logarithmic on the Higgs mass. Fits to data available before summer 1995, including the combined CDF and D0 value $m_{top} = 181 \pm 12$ GeV [24], the LEP value of $R_b = 0.2204 \pm 0.0020$ and the new SLAC-95 value of A_{LR} giving $\sin^2\theta_{eff}(A_{LR}) = 0.2305 \pm 0.0005$ (combined 1994 + 95), are shown in Fig. 7a [25]. The minimum χ^2 is obtained for $m_H \sim 100$ GeV, but it is shallow and the upper limit of m_H is not stringent. More exactly, this analysis gives $m_H = 76\ ^{+152}_{-50}$ GeV and the 95% C.L. upper bound is $m_H \leq 0.7$ TeV. A reanalysis including LEP data from summer 1995 does not change significantly the best value of m_H, although there is a significant degradation of the best χ^2 due to R_b, R_c [25]. If errors on R_b, R_c are arbitrarily increased by a factor 3, the optimal m_H increases by ≈ 45 GeV, well within the uncertainty of the fits. Very similar fits are obtained by the LEP electroweak working group [26]. A best χ^2 is consistently obtained for $m_H \sim 100$ GeV and a $\Delta\chi^2 = \chi^2 - \chi^2_{min} < 4$ limit for $m_H < 0.85$ TeV. Thus a broad mass range must be explored in future experiments. The present lower bound from LEP is $m_H \geq 65$ GeV [27] and LEP2 should allow to extend the search to ≈ 90 GeV. Figure 7b shows the allowed regions for m_{top} and m_H [28], the contours indicating the scale up to which the SM is supposed to be valid; the region to the right is excluded by the top rad. corrections destabilizing the Higgs potential. If there is no new physics before the GUT scale, m_H is limited to ~ 200 GeV; for a lower breakdown scale m_H could be as large as ~ 0.5 TeV. From these bounds and the (high) measured value of m_{top}, if a Higgs signal were found at LEP2, it is unlikely to be the SM one, i.e. new physics would be at a TeV scale, possibly supersymmetry, a most interesting prospect for the LHC.

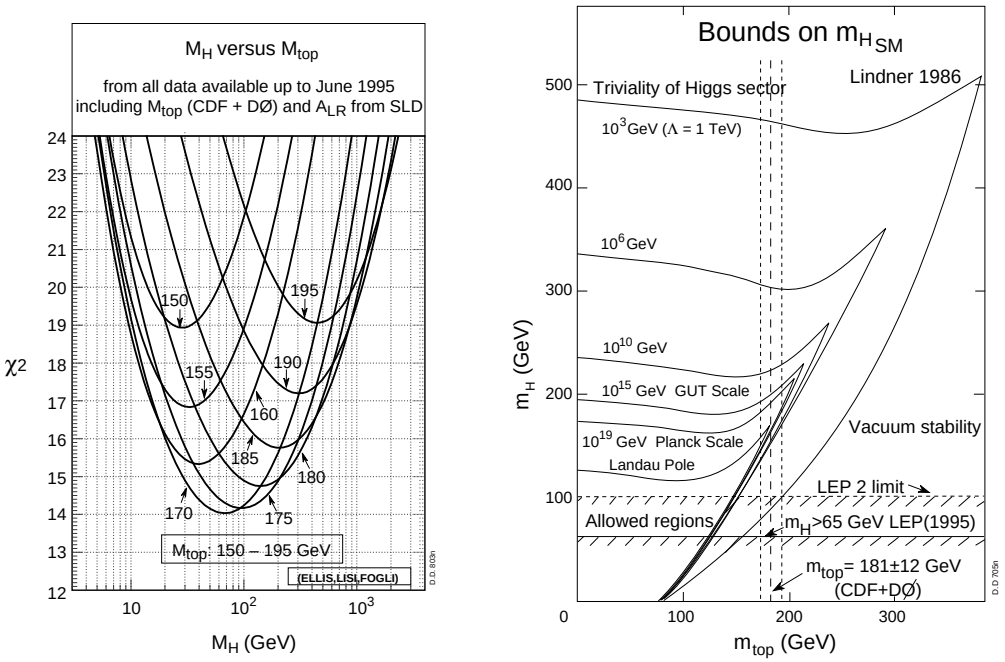

Fig.7a : χ^2 as a function of m_H for various m_{top} values [25].

Fig. 7b: Bounds on the top and SM Higgs masses from ref. [28]; the allowed region extends from the lower left corner up to the indicated scale of assumed SM break-down.

ATLAS and CMS have been designed to allow investigations over the entire mass range up to ~1TeV. For the $80 < m_H < 140$ GeV domain the $H \rightarrow \gamma\gamma$ decay mode provides the best chances. Supporting evidence could be obtained from $H \rightarrow b\bar{b}$ for $m_H < 100$ GeV [4]. This mass range is most important as it connects to the LEP domain and, as discussed later, if the lightest MSSM Higgs boson exists, it must be within $m_h < 130$ GeV. For $130 \leq m_H \leq 700$ GeV the channel $H \rightarrow ZZ^*$, $ZZ \rightarrow 2\,l^+2l^-$ is the most appropriate one. For $m_H > 650$ GeV the difficulties increase as the Higgs becomes broader and the cross-section decreases. We discuss in more detail these points, in particular the rad. correction favored $m_H < 300$ GeV range which is also more demanding in terms of detector performance and versatility.

$H \to \gamma\gamma$

For $H \to \gamma\gamma$ let us use the CMS study [17]. The cross section $\sigma \cdot B(H \to \gamma\gamma)$ for $\sqrt{s}$ = 14 TeV is 76 (68) fb for m_H = 110 (130) GeV. The photon acceptance is $|\eta| < 2.5$, and the transverse momentum cuts $p_t^{\gamma_1} > 40$ GeV, and $p_t^{\gamma_2} > 25$ GeV. The background to $H \to \gamma\gamma$ is made of: i) prompt di-photon production from quark annihilation and gluon fusion, ii) prompt di-photon production from bremsstrahlung from the quark line, and iii) reducible background from jets or from jets + 1 prompt photon, with a leading π^0 (or η) decaying to $\gamma\gamma$. At $m_{\gamma\gamma}$ = 110 GeV for example, the cross-sections $d\sigma / dm_{\gamma\gamma}$ are 84 fb / GeV for isolated bremsstrahlung, 61 fb / GeV for quark annihilation and 72 fb / GeV for gluon fusion. The jet and bremsstrahlung backgrounds can be reduced by a photon isolation cut. Photons from π^0s in the $p_t \sim 50$ GeV range are separated in the calorimeter by ~1 cm. The presence of two impacts can be detected using a lateral shower profile in the calorimeter, or the preshower. The jet-jet and jet-γ backgrounds are reduced to < 15% of the irreducible $\gamma\gamma$ background by photon isolation and π^0 rejection cuts [3]. An efficiency of 64% is assumed for the reconstruction of each photon; this accounts for conversion, fiducial volume, isolation and π^0 rejection losses. Subsequent studies have shown that about 50% of conversions could be recovered thus an efficiency of 74% would at present seem more appropriate [29].

Figure 8a shows a background-subtracted $\gamma\gamma$ effective mass plot for an integrated luminosity of 10^5 pb^{-1} taken at high luminosity with expected signals at 90, 110, 130 and 150 GeV. The crystal calorimeter is assumed to have an energy resolution of $\Delta E/E = 2\%/\sqrt{E} \oplus 0.5\% \oplus 0.200/E$ in the barrel and of $5\%/\sqrt{E} \oplus 0.5\% \oplus 0.200/E$ in the barrel and endcap regions where there is a preshower detector. The $\gamma\gamma$ mass resolution at $m_{\gamma\gamma}$ = 110 GeV is 870 MeV. Figure 8b shows the level of σ.B required to have a specified signal significances $\left(N_S / \sqrt{N_B}\right)$ as a function of mass with the performance and selection cuts of CMS. The expected σ.B for the SM Higgsis also shown; the uncertainty on this prediction is ~ ± 15% due to structure functions alone and the uncertainty due to 'k factors' is comparable. From Fig. 8b we conclude that with 10^5pb^{-1} the SM Higgs could be discovered with > 5σ signal significance across the range 90 to 150 GeV. A significant advantage of the potentially excellent resolution is that in the 10^{33} cm^{-2}s^{-1} regime where the resolution is best (known vertex), with a reduced luminosity of $3\text{x}10^4$ pb^{-1} the mass range ≈ 95 to 140 GeV could be covered.

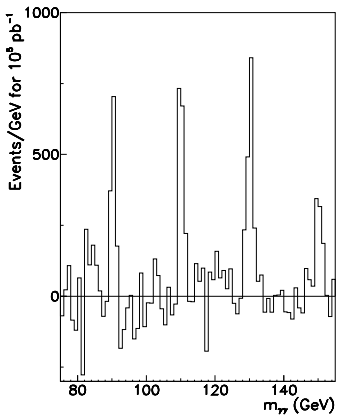

Fig. 8a: Background-subtracted 2γ mass for 10^5 pb^{-1} with signals at m_H = 90, 110, 130 and 150 GeV in the $PbWO_4$ calorimeter.

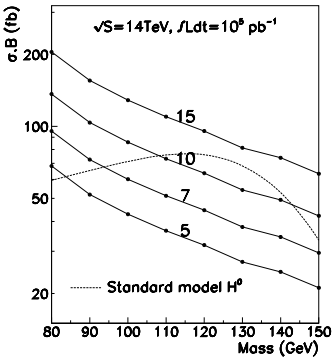

Fig. 8b: Signal significance contours for 10^5 pb^{-1} taken at high luminosity.

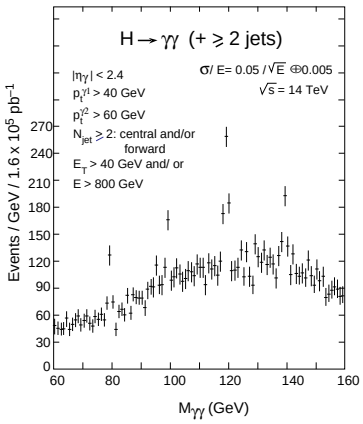

Fig. 8c: Reconstructed $H \to \gamma\gamma$ signal in a crystal calorimeter for H produced in association with hard jets for 1.6×10^5 pb^{-1}.

In the inclusive $H \to \gamma\gamma$ search the signal to background ratio is ~ 1/10. This can be improved using Higgs production in association with hard jets or isolated leptons. This is more demanding in terms of statistics, but is significantly less demanding in terms of calorimeter performance, intrinsic energy resolution or calibration and there is no need for a preshower. Sources of such events are radiative corrections to $gg \to H$ with hard real gluons, associated production of $t\bar{t}H$, WH, ZH and WW (ZZ) fusion. Figure 8c shows the signal for m_H = 80, 100, 120, 140 GeV superimposed on the background in a search where at least two hard jets are demanded [30]. The number of signal events is about 100 for 1.6×10^5 pb^{-1}, an order of magnitude less than

in the inclusive $\gamma\gamma$ search, but the signal-to-background ratio is ~1. Signal significance is ≈ 7 to 14σ depending on m_H. A similar analysis is possible requiring a hard and isolated lepton [3,4]. The hard jets or lepton present in the event indicate the interaction vertex at any luminosity and could dispense us of a use of a preshower. The drawback is the uncertainty in Higgs production at high p_t and even more so for the backgrounds [30].

$H \rightarrow ZZ^*$, $ZZ \rightarrow 4$ Charged Leptons

The four-lepton channel allows to search the $m_H \approx 130$ to ~ 800 GeV range. For $m_H < 2m_Z$ one of the Z's is off-mass-shell and the backgrounds are $t\bar{t}$, $Z b\bar{b}$ and ZZ*. The ZZ* background is irreducible, $Z b\bar{b}$ can be suppressed by lepton isolation and lepton impact parameter cuts and $t\bar{t}$ by a Z mass cut and lepton isolation or impact parameter cuts [31]. The signal cross sections are $\sigma \cdot B = 2.9$, 5.3 and 1.4 fb for $m_H = 130$, 150 and 170 GeV respectively. For $m_H < 200$ GeV the width of the Higgs is small, $\Gamma_H < 1$ GeV, and the signal significance is sensitive to the mass resolution. In CMS the $Z \rightarrow \mu^+\mu^-$ resolution is $\sigma_Z = 1.6$ GeV and the $H \rightarrow 2\mu^+2\mu^-$ resolution $\sigma_H = 0.9$ GeV for $m_H < 200$ GeV [32]. Internal bremsstrahlung effects are included and detailed GEANT simulations are performed to investigate the effects of external bremsstrahlung for electrons [21]. With a 5×7 crystal matrix to reconstruct electrons, the mass resolution for $Z \rightarrow e^+e^-$ is 2.2 GeV, and the mass resolution for $H \rightarrow ZZ^* \rightarrow 2e^+2e^-$ is 2.0 GeV.

The selection cuts for electrons are: one with $p_t > 20$ GeV, one with $p_t > 15$ GeV, and the remaining two with $p_t > 10$ GeV; for muons the pcuts are 20, 10 and 5 GeV. There is a certain flexibility in the ways to suppress $t\bar{t}$ and $Z b\bar{b}$ backgrounds using the Z mass cut, lepton isolation or lepton impact parameter cuts according to the m_H range investigated, detector performance and instantaneous luminosity [31]. Figure 9a shows the reconstructed Higgs signals at 130, 150 and 170 GeV for 10^5 pb^{-1}. Figure 9b shows the σ.B required to obtain a given signal significance with CMS performance and cuts, compared to the expected σ.B in the SM. The mass range covered goes from ≈ 120 GeV up to $2m_Z$. Observation of the signal in the vicinity of $m_H = 165$ GeV (opening of the $H \rightarrow WW$ decay channel) is difficult and requires 10^5 pb^{-1} for a 5σ significance signal. Figure 10 shows the results of a similar study made for the ATLAS detector [4].

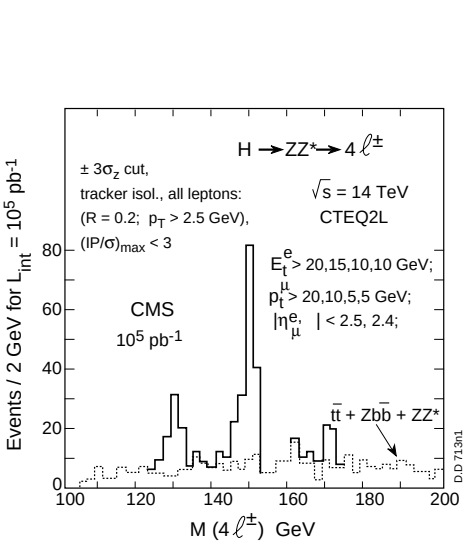

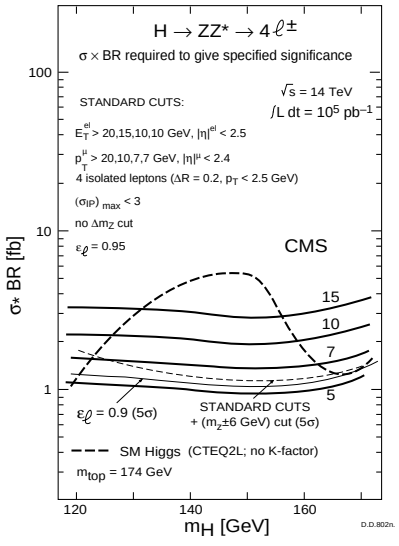

Fig. 9a: Reconstructed signals for $m_H = 130$, 150 and 170 GeV in the $4l^{\pm}$ channel for 10^5 pb^{-1} in CMS.

Fig. 9b: σ.B required to obtain a given signal significance with CMS performance and cuts, compared to the expected σ.B in the SM.

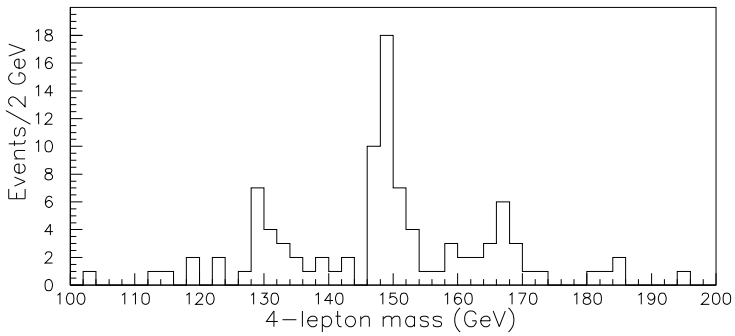

Fig. 10: Reconstructed four lepton signals for m_H= 130, 150 and 170 GeV for 3×10^4 pb^{-1} in ATLAS.

For $m_H > 2m_Z$ the main background is non-resonant ZZ production. The p_t and η selection cuts are the same as for the $H \rightarrow ZZ^*$ channel and the effects of internal and external bremsstrahlung are treated the same way [21]. Two $e^+ e^-$ or $\mu^+ \mu^-$ pairs consistent with a Z mass are required. The Z mass window can be large since there are no backgrounds which are critically affected by the two-lepton mass cut. Lepton isolation cuts are not needed as the $t\bar{t}$ background is negligible. Figure 11 shows the expected 4-lepton mass spectrum for several m_H values. Figure 12a summarizes the expected $H \rightarrow ZZ^*$, ZZ signal significance for several integrated luminosities. With 10^4pb^{-1}, the 5σ discovery region extends from ≈ 135 to 155 GeV and from $2m_Z$ up to m_H ≈ 400 GeV. Figure 12a also shows the effect of varying the input structure functions. With 10^5pb^{-1} the upper mass reach is ≈ 650 GeV, but it can be extended to ≈ 800 GeV with a more carefull choice of selection criteria exploiting the scalar nature of the Higgs and the longitudinal polarisation of decay Z's, Figs. 11c and 12b [33].

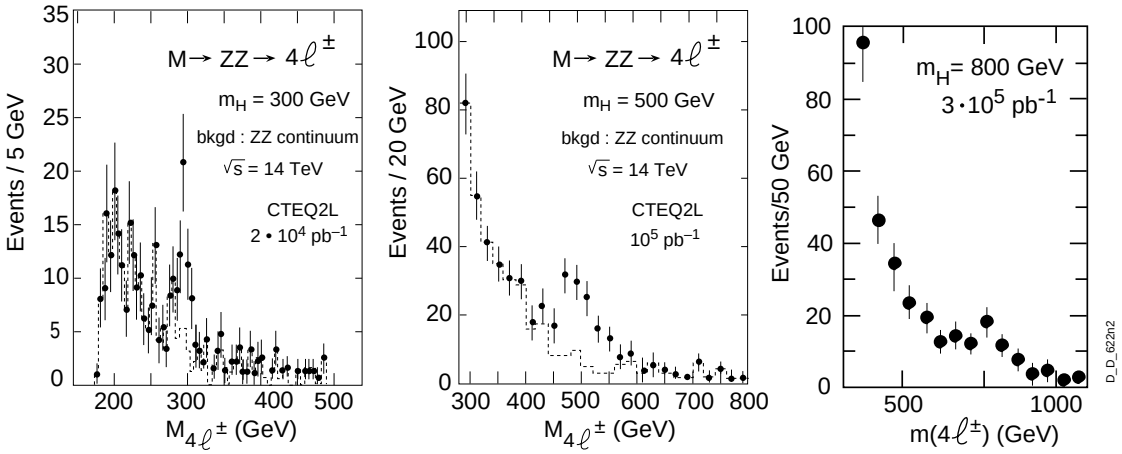

Fig.11: The four-lepton mass distributions from $H \rightarrow ZZ \rightarrow 4\, l^{\pm}$s and the ZZ continuum background for m_H= 300 and 2×10^4 pb^{-1}, m_H= 500 GeV with 10^5 pb^{-1} and m_H = 800 GeV with 3×10^5 pb^{-1} in CMS.

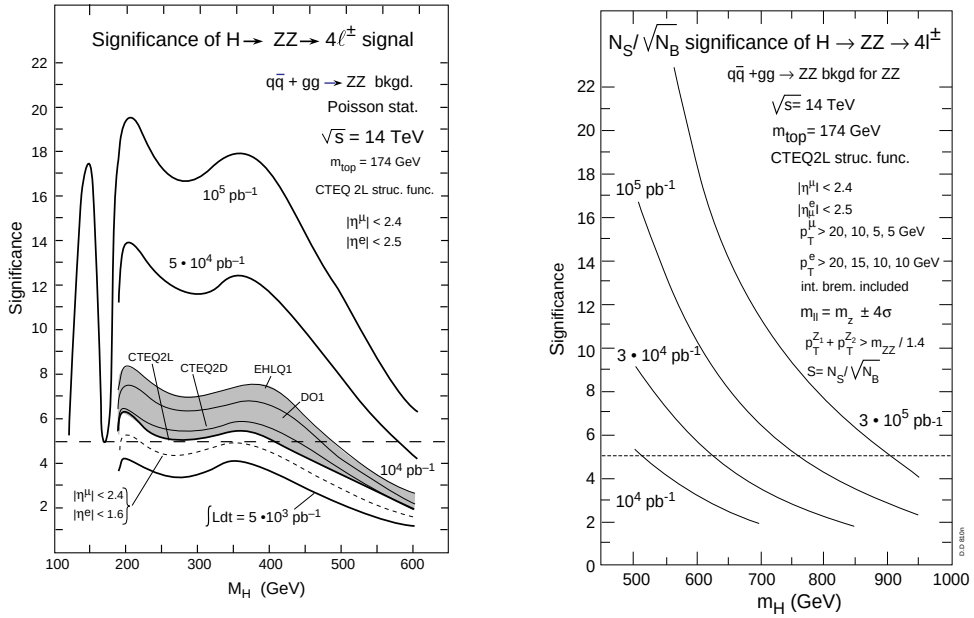

Fig. 12a: Significance of H →ZZ*, ZZ → 4$l^{\pm}$ signals as a function of m_H for integrated luminosities from 5×10^3 to 3×10^5 pb^{-1}; Fig. 12b is for cuts optimized for the high mass range.

H → *ll*νν

To explore the $m_H \sim 1$TeV region decay modes with larger branching ratio must be used. The channel H → *ll*νν has a six times larger branching ratio than H →4 $l^{\pm}$ and a distinct signature: two high p_t leptons from the Z decay and high E_t^{miss}. For $m_H > 500$ GeV, the signal is a broad Jacobian peak in the two-lepton transverse momentum distribution. The main background channels are ZZ, ZW, $t\bar{t}$ and Z + jets. For masses beyond ~700 GeV the signal becomes less distinct, as the Higgs width increases rapidly. Only a precise knowledge of background would allow the unambiguous observation of such a signal. To suppress backgrounds forward jets from WW (ZZ) fusion production can be used as an additional signature. Details on such an analysis can be found in [34]. Figure 13 shows the expected signal for $m_H = 800$ GeV and 10^5 pb^{-1}. This channel would allow discovery of a SM Higgs up to 1 TeV with an integrated luminosity of 10^5 pb^{-1}. Figure 14 shows the results of a similar analysis done for the ATLAS detector [34].

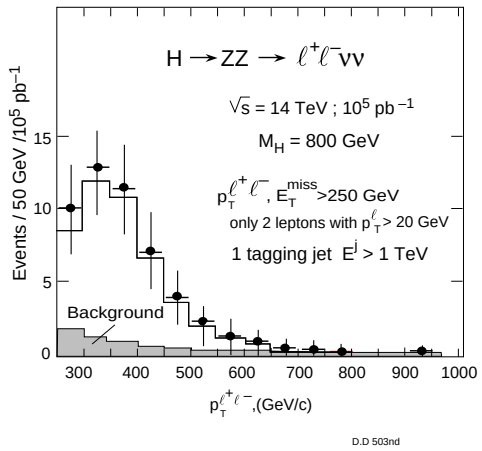

Fig. 13: H → l^+l^-νν signal for m_H= 800 GeV and 10^5 pb^{-1} in CMS. One tagged jet with E > 1 TeV is assumed.

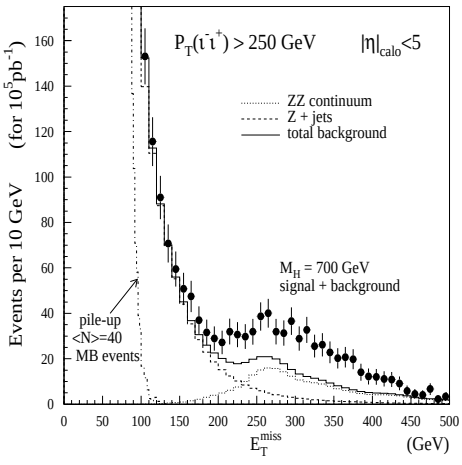

Fig. 14: H → l^+l^-νν signal for m_H= 700 GeV and 10^5 pb^{-1} in ATLAS, the various background components are shown separately.

$H \rightarrow WW \rightarrow l\nu jj$ and $H \rightarrow ZZ \rightarrow llqq$

These decay channels are needed to search the $m_H \approx 1$ TeV region exploiting the large W, Z $\rightarrow q\bar{q}$ branching ratios. The signature is a high p_t lepton pair with $m_{ll} \approx m_Z$, for $H \rightarrow ZZ$, or a high p_t lepton plus large E_t^{miss} for $H \rightarrow WW$. In addition, hard central jets from the hadronic decays of Z / W, with $m_{jj} \approx m_{W/Z}$ are required. The main backgrounds are Z + jets, ZW, ZZ for $H \rightarrow ZZ$, and W + jets, $t\bar{t}$, WW, WZ for $H \rightarrow WW$. In this mass range the Higgs is very broad ($\Gamma_H \approx 0.5$ TeV for $m_H \approx 1$ TeV) and indistinct in effective mass distributions. The forward 'tagging jets' can improve the signal to background ratio as WW / ZZ fusion represents about 50% of the cross-section. A set of appropriate cuts can be found in [34]. Figure 15 shows the expected $H \rightarrow WW \rightarrow l\nu_t jj$ signal for 3×10^4 pb^{-1}; one expects ≈ 22 signal events over a background of ≈ 8 events for m_H = 1 TeV, giving a 4σ signal significance. Simultaneous observation in the $llqq$, $l\nu qq$ and $ll\nu\nu$ channels would give a ≈ 5.5σ signal for 3×10^4 pb^{-1}.

Overview of SM Higgs detection possibilities

Figure 16 summarizes the mass range each mode would allow to investigate. The entire SM Higgs mass range can be covered with some safety margin. For the 80-200 GeV range high performance and high integrated luminosity are needed. Most demanding is the 80-130 GeV range, the detection of $H \rightarrow \gamma\gamma$ justifying the $PbWO_4$ calorimeter. The calorimeter performance is critical, resolution, calibration and monitoring will be of decisive importance. If a $\gamma\gamma$ resolution better than 1 GeV is achieved, few$\times 10^4$ pb^{-1} can be enough for discovery in the inclusive $\gamma\gamma$ search. In case of insufficient performance, say effective resolution ~2GeV, we must resort to the $\gamma\gamma$ +lepton, or $\gamma\gamma$ + multijets subchannels instrumentally less demanding, but requiring in excess of 10^5pb^{-1}. For the ~130-200 GeV domain muon and electron resolution and acceptance will be critical. Relaxing the m_Z cut and compensating with lepton isolation and impact parameter cuts, masses down to 120 GeV are accessible. There is a window at $m_H \approx 165 \pm 5$ GeV where 10^5 pb^{-1} are mandatory for 5σ signal significance. For $m_H >$ 650 GeV the difficulties increase and excellent knowledge and control of backgrounds will be of decisive importance. The performance of the hadron calorimeter and detector hermeticity are critical. An integrated luminosity of $\approx 10^5$ pb^{-1} is needed to cover the upper m_H range. If the SM Higgs conforms to present expectations it should not escape detection at the LHC.

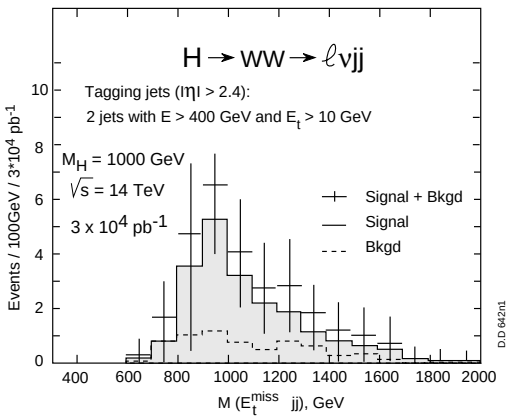

Fig.15: Higgs signals in $H \rightarrow WW \rightarrow l\nu jj$ for m_H = 1 TeV and 3×10^4 pb^{-1}.

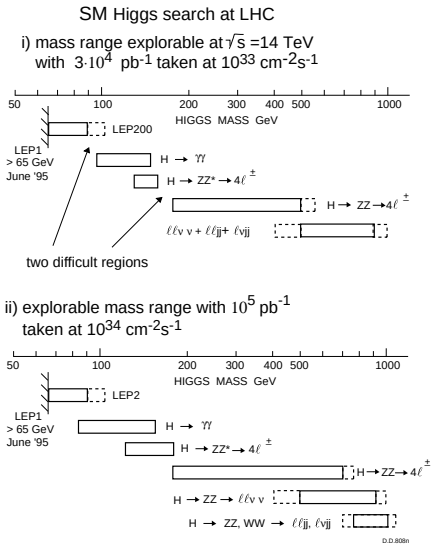

Fig.16: Overview of Standard Model Higgs observability at LHC versus luminosity

3.2 Searches for MSSM Higgs bosons

The difficulties of the SM Higgs scenario are alleviated in SUSY theories at the expense of introducing several Higgs bosons. The Minimal Supersymmetric Standard Model (MSSM) contains one charged ($H^{\pm}$) two CP-even (h, H) and one CP-odd (A) state. The specific scenario that has been investigated by ATLAS and CMS is the one of ref. [6] with a heavy mass scale at 1 TeV. The decay channels of the MSSM neutral Higgs bosons are similar to the S M Higgs, but the production rates are significantly modified by MSSM couplings. Particularly interesting is the the light scalar h whose mass is bounded by $m_h < m_Z$ at lowest order; radiative corrections modify this upper bound to $m_h < 130$ GeV [6, 35]. Thus the h could be outside the reach of LEP2 limited to $m_h < 90$ to 100 GeV. This puts additional emphasis on the $h \rightarrow \gamma\gamma$, $b\bar{b}$ and ZZ* searches at LHC to test this clear prediction of the MSSM. The present LEP experimental mass limit on m_h are > 65 GeV for tgβ = 1, >45.5 GeV for moderate tgβ (10 to 20) and > 55 GeV for large tgβ [27].

h,H $\rightarrow \gamma\gamma$

The MSSM Higgs bosons h,H are extremely narrow in the kinematic regions for which the $\gamma\gamma$ decay has a useful branching ratio. The experimental requirements and expected backgrounds are the same as in the SM H $\rightarrow \gamma\gamma$ search. From the Higgs mass and $\sigma \cdot B$ as a function of m_A and tanβ, the significance of a possible h,H $\rightarrow \gamma\gamma$ signal can be extracted from Fig. 8b. Figure 17 shows several contours in the (m_A, tanβ) plane, a 5σ discovery contour for $10^5 pb^{-1}$ taken at high luminosity, a 3σ exclusion contour for same conditions, and a 5σ discovery contour for $3x10^4 pb^{-1}$ taken at $10^{33} cm^{-2} s^{-1}$. The region of (m_A, tanβ) parameter space which can be explored with LEP2 at $\sqrt{s}$ = 190 GeV and 500 pb^{-1} (assuming the heavy mass scale at 1 TeV) is also shown. The two machines, LHC and LEP2, are complementary in their possibilities, LHC being sensitive at large tgβ, large m_A and LEP2 at low tgβ or low m_A.

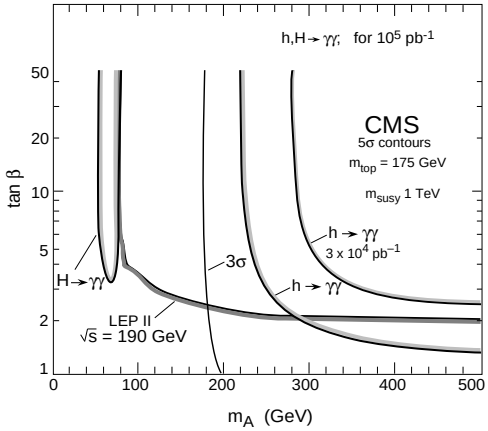

Fig. 17: Significance contours in the MSSM parameter space for h,H $\rightarrow \gamma\gamma$ signals in CMS. The region explorable at LEP2 is also shown. The explorable regions are inside the shaded boundaries.

H $\rightarrow$ ZZ*, ZZ and h $\rightarrow$ ZZ*

The H and h bosons couple to W and Z pairs and can be searched in h, H $\rightarrow$ ZZ*, ZZ $\rightarrow 4l^{\pm}$. Radiative corrections have a large effect on the upper bound of m_h, and the opening of the h $\rightarrow$ ZZ* channel is possible only if m_h exceeds ≈120 GeV. Representative values of $\sigma \cdot B$ for H $\rightarrow$ ZZ*, ZZ$\rightarrow 4l^{\pm}$ and h $\rightarrow$ ZZ* $\rightarrow 4l^{\pm}$ are given in Table 1. The simulation procedure and experimental criteria are the same as for the SM H $\rightarrow$ ZZ*, ZZ. Both the h and H are narrow, with widths well below 1 GeV in the accessible parameter range. The regions of MSSM parameter space in which the h and H can be looked for via ZZ*/ZZ are disconnected, a low tanβ region for H and a high tanβ region for h. The 5σ discovery limits in these two channels are shown in Fig. 18a for $10^5 pb^{-1}$. The limits of the h $\rightarrow$ZZ* discovery region are very sensitive to changes in m_h, the contour in Fig. 18a is for m_{top} = 174 GeV and m_h calculated with one-loop radiative corrections giving $m_h < 128$ GeV [36].

Table 1. $\sigma \cdot B$ (fb) for $H \rightarrow ZZ^*$, ZZ, $h \rightarrow ZZ^*$ for different MSSM parameter values.

	m_A = 80 GeV	m_A = 150 GeV	m_A = 200 GeV	m_A = 300 GeV
$H \rightarrow ZZ$ ($\tan\beta = 2$)	2.2	1.6	1.8	1.2
$h \rightarrow ZZ^*$ ($\tan\beta = 10$)	0.01	1.3	1.7	1.6

h, H, A $\rightarrow \tau\tau \rightarrow l^{\pm} + h^{\pm} + X$

The $\tau\tau$ final states can be looked for in lepton + hadron or e+ μ channels. As there are several neutrinos in the final state, mass peaks are difficult to reconstruct and evidence for a signal comes mainly from an excess of events over expected SM backgrounds. Backgrounds are due to Z, $\gamma^* \rightarrow \tau\tau$, $t\bar{t} \rightarrow \tau\tau$ +X, τ+X and $b\bar{b} \rightarrow \tau\tau$+ X, τX, and to events with one hard lepton and jets with a jet misidentified as a τ. Event selection algorithms have been developed requiring : i) one isolated lepton, ii) one τ-jet candidate and iii) no other significant jet activity in the event [3,4,37]. The $\tau \rightarrow$ charged hadron decay is selected by requiring a collimated high E_t jet in the calorimeters and exactly one high p_t charged track within $\Delta R < 0.1$ of the calorimeter jet axis. The small Q-value of the τ decay allows reconstruction of m_A, if A has a transverse boost, by taking the neutrinos parallel with the hadron and the lepton. The reconstructed mass distribution has a mass resolution of ~ 15 GeV for m_A = 100 GeV [4]. The 5σ discovery contours in the (m_A, $\tan\beta$) plane for A, H, $h \rightarrow \tau\tau \rightarrow l^{\pm}$+ $h^{\pm}$ and A, H, $h \rightarrow \tau\tau \rightarrow$e+ μ are shown in Fig. 18a for $10^4 pb^{-1}$. The $\tau\tau$ decay modes allow the exploration of a substantial region of MSSM parameter space.

Charged Higgs $H^{\pm}$ in $t \rightarrow H^{\pm} b$, $H^{\pm} \rightarrow \tau\nu_\tau$

In the MSSM the top quark can decay to a charged Higgs, $t \rightarrow H^+b$. The $t \rightarrow H^+b$ branching ratio is complementary to the $t \rightarrow Wb$ one, it is large at low and high $\tan\beta$ values, having a minimum at $\tan\beta \approx 6$. The H^+ has two main decay modes, $H^+ \rightarrow c\bar{s}$ and $H^+ \rightarrow \tau\nu_\tau$. The $H^+ \rightarrow \tau\nu_\tau$ branching ratio is large, ≈ 98%, for $\tan\beta >$ 2, and only slightly dependent on $\tan\beta$. Studies have been made [3,4,38] of the observability of the $H^{\pm}$ signal from $t\bar{t}$ events where one top decays leptonically and the other to a charged Higgs followed by $H^+ \rightarrow \tau\nu$ using the one-prong τ signature. The existence of H^+ in the data can only be inferred from an excess of τ production over what is expected from the SM backgrounds. Irreducible ones involve real τ's as in $t\bar{t}$ with $t \rightarrow Wb$, $W \rightarrow \tau\nu_\tau$, reducible ones are from $t\bar{t}$, where a W decay jet fakes a τ, or a b-jet gives a real or a fake τ candidate, and from $b\bar{b}$. The main selection criteria are i) an isolated high p_t lepton and ii) one jet with $E_t > 40$ GeV fulfiling the τ selection criteria. To suppress the dominant W + jet background at least one tagged b-jet is required in the event [38,39]. One contour in Fig. 18a shows the (m_A, $\tan\beta$) region that can be explored with $t \rightarrow H^{\pm}b$ at 5 σ significance with 10^4 pb^{-1} integrated luminosity.

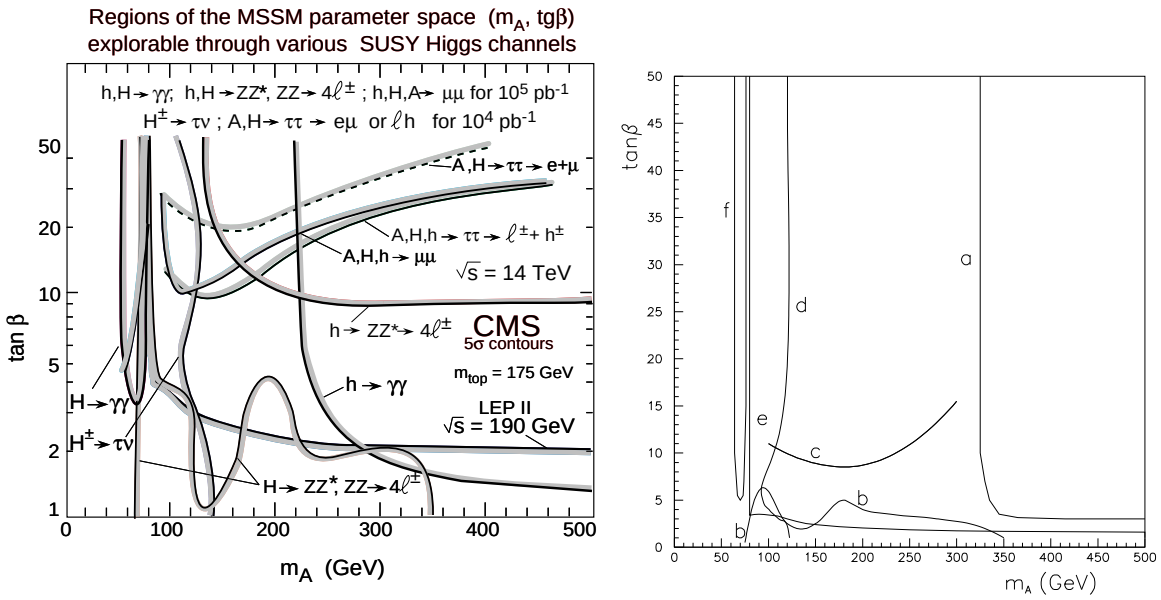

Fig. 18a: Significance contours (5σ) in the MSSM parameter space for different Higgs boson decays accessible to CMS. The region explorable at LEP2 with 500 pb^{-1} is also shown. The explorable regions are inside the shaded boundaries. Fig. 18b: Same analysis in ATLAS: contours a) $h \rightarrow \gamma\gamma$, b) $H \rightarrow ZZ \rightarrow 4l^{\pm}$, c) $A \rightarrow \tau\tau$, d) $t \rightarrow H^{+}b$, e) LEP2 sensitivity and f) $H \rightarrow \gamma\gamma$,; c) and d) are for $10^4 pb^{-1}$ a), b) and f) are for $10^5 pb^{-1}$.

h, H, A $\rightarrow \mu\mu$

In both the SM and MSSM the branching ratio of $H \rightarrow \mu\mu$ is small, about 3×10^{-4}. For the SM Higgs the $\mu\mu$ channel is overwhelmed by the large Drell-Yan background. In the MSSM, however, the cross-sections are enhanced relative to the SM at large tg. An appropriate set of signal selection cuts is: i) two muons with $p_t^{\mu} \geq$ 10 GeV and ii) no more than one jet with $E_t \geq 40$ GeV within $|\eta| \leq 2.4$ [40]. Figure 19 shows the signal for two values of m_A and large tgβ. The h and A mass peaks remain unresolved when $m_A \leq 130$ GeV, and similarly the A and H peaks cannot be separated for $m_A \geq 130$ GeV. The peaks become resolvable at tanβ values $\approx 10 - 15$. Close to the Z-peak the signal is difficult to observe as it sits on the shoulder of the much larger Z-peak, but the signal-to-background ratio can be improved by b-tagging [39]. Whilst $gg \rightarrow b\bar{b}H$ associated production is negligible for the SM Higgs compared to $t\bar{t}H$, in the MSSM the rate of $gg \rightarrow b\bar{b}H_{SUSY}$ is~50% of the total production rate for $m_A \sim 100$ and increases with m_A (tanβ = 10 – 30). B-taggingthus favours $b\bar{b}$ H_{SUSY} production relative to Z $b\bar{b}$ which amounts to only few percent of Z + jets [3]. The 5σ discovery contour for H, h, A $\rightarrow \mu\mu$ for an integrated luminosity of 10^5 pb^{-1} is shown in Fig. 18a. It is close to the H, h, A $\rightarrow \tau\tau$ contour for 10^4 pb^{-1}, but the $\mu\mu$ channel provides a much better signal identification and mass resolution.

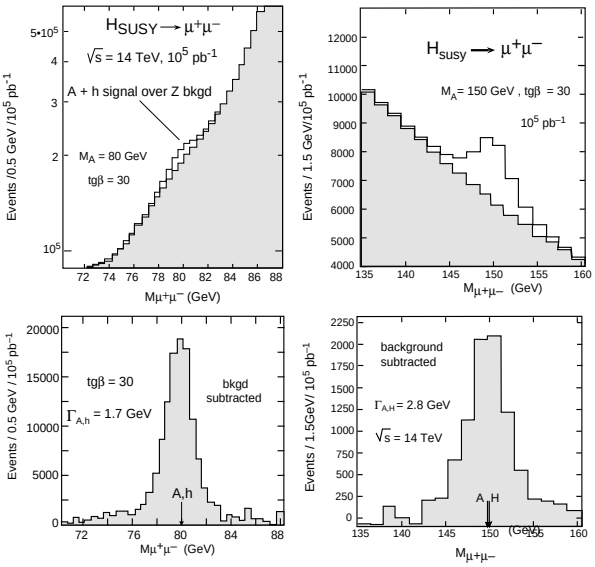

Fig. 19: Inclusive $H_{SUSY} \rightarrow \mu\mu$ at $\tan\beta = 30$ for $m_A = 80, 150$ GeV and $10^5 pb^{-1}$. The h, A and H, A masses are almost degenerate.

Conclusions on SUSY Higgs Searches

Figure 18a summarises investigations done by CMS on the regions of MSSM parameter space that can be explored using various channels with luminosities ranging from $10^4 pb^{-1}$ to $10^5 pb^{-1}$. Figure 18b shows the results of a similar study done by ATLAS [4]. There are regions of parameter space that are explorable through several channels. This may eventually allow clarification as to which of the various SUSY models is correct, if any. Figures 18 also show the region of parameter space which can be explored with LEP2 at $\sqrt{s} = 190$ GeV. LEP2 and LHC clearly complement each other. With the channels investigated in detail up to now and with $10^5 pb^{-1}$ there remains, however, a region inaccessible to both machines given approximately by $110 < m_A < 220$ GeV, $2.5 < \tan\beta < 10$. A channel which could at LHC shed light on this region is h, $H \rightarrow b\bar{b}$, from Wh, Zh and $t\bar{t}h$ final states [41]. The pixel detectors included in both ATLAS and CMS tracking system may allow this, but more work is needed to evaluate how realistic is this possibility. Another way to cover most of this region would be to accumulate > 3x $10^5 pb^{-1}$ [4]. The LEP2 contour could also be much more favourable if the energy could be increased to ≈205 GeV as then the horizontal branch of the LEP2 coverage would reach up to $tg\,\beta \approx 8$ with $300 pb^{-1}$, but this may be financially unafordable. If the stop-quark mass, or more generally the heavy mass scale of MSSM were lower than the 1 TeV assumed here, the LEP2 coverage would improve in the same way [6].

3.3 SUSY searches

Physics performance studies for signals other than the MSSM Higgs bosons have not been performed to the same depth. A general squark/gluino signal detection capability has been tested, but a systematic exploration of model parameter space has not yet been done, partly due to the great variety of scenarios to be investigated, but mainly because it is sensitive to detector E_t^{miss} resolution which is a global variable requiring a realistic simulation of the entire calorimetric system. The tail of the E_t^{miss} distribution is affected by geometrical coverage, cracks and gaps due to mechanical structures, cable and cooling system passages etc, thus a reliable E_t^{miss} response of a detector can come only late in the detector design phase.

The present lower mass bound on squark and gluino masses from Tevatron experiments is 212 GeV if $m_{squark} = m_{gluino}$, and $m_{gluino} > 179$ GeV if $m_{squark} >> m_{gluino}$ [42]. CDF and D0 should be able to explore masses up to ~ 0.4 TeV, beyond that is the LHC domain. Studies done in ATLAS and CMS on the benchmark jets + E_t^{miss} channel concern the squark/gluino upper mass reach which, depending on the scenario, is ~2 TeV for $10^5 pb^{-1}$ [3,4]. This channel is fed, for example, by squark or gluino pair production followed by $\tilde{q}_R \rightarrow q\chi_1^0$

or $\tilde{g} \rightarrow q\bar{q}\chi_1^0$ decays. No mass peaks can be expected in these searches and evidence for a signal depends on an excess of events over expected backgrounds. For high gluino/squark masses the E_t^{miss} due to signal neutralinos and to neutrinos from SM backrounds $t\bar{t}$, W($\rightarrow$ lν)+jets, Z($\rightarrow \nu\nu$)+jets, dominates over the instrumental E_t^{miss} from detector response to jets. The lower mass reach, at the junction between the FERMILAB and LHC search regions, has not been so reliably explored yet, as QCD multijet events are here the dominant backround [3]. The production cross sections are large, however, and significant searches will be possible already with $10^3 pb^{-1}$[3,4,43]. Figure 20 shows expected squark and gluino signals, with masses 0.5 to 1.5 TeV, in the jets + E_t^{miss} final states. Selection criteria are at least three hard jets of E_t > 200 GeV and high circularity C > 0.2 [43]. The expected instrumental (jets) and $t\bar{t}$, W, Z backgrounds are shown separately. Another experimental signature that has been studied is leptons + E_t^{miss} + jets. These final states are fed by cascade decays of squarks or gluinos through $\chi_i^{\pm}$ and χ_i^0 decaying to leptons. Studies of gluino pair production have been performed for final states with one, two and three high p_t muons. Two same-sign isolated muons are a particularly clean signature. These channels allow to explore the ~0.3 to 1.5 TeV gluino mass range [3,44]. Through the internal SUSY mass relations [5,35] the exploration of the ~TeV squark/gluino mass range would provide also a very significant constraint on, or in case of discovery provide indirect evidence for the cosmologically relevant LSP-lightest neutralino for a mass up to ~ 0.2 TeV.

A comprehensive phenomenological study of the explorable regions of supergravity constrained MSSM parameter space exploiting the E_t^{miss}+ multijets, leptons + E_t^{miss} + jets final states from gluino and squark production, and the two and three-leptons + E_t^{miss} final states from slepton and chargino, neutralino production has been performed in ref. [5] assuming a generic LHC detector response. The results are shown in Fig. 21. They seem to indicate that with $10^4 pb^{-1}$ most of parameter space of this particular model could be explored. These very encouraging results have to be eventually substantiated with more detailed and realistic detector response simulations.

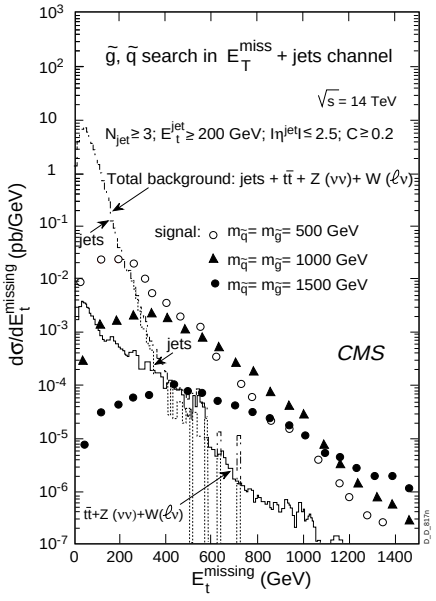

Fig. 20: E_t^{miss} distributions for squark and gluino signals and expected backgrounds in CMS.

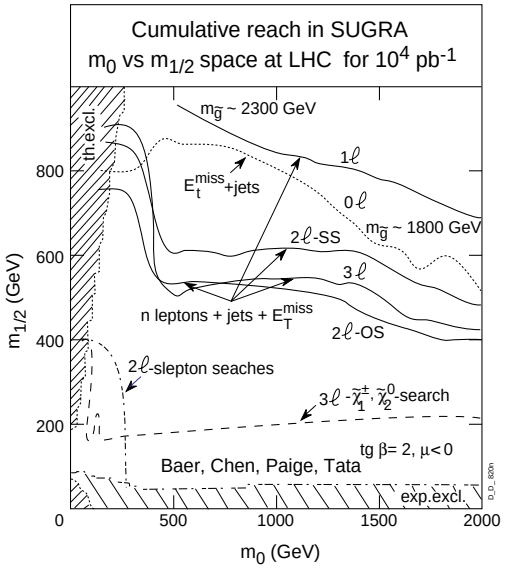

Fig. 21: SUSY parameter space explorable through different channels, from ref. [5].

3.4 B - Physics at the LHC

The main issue in B-physics is the observation of CP-violation. For such a measurement high statistics are vital as the interesting decay modes have small branching ratios (~10^{-5}) and the large B-production rate of a hadron collider is essential. At LHC ~10^{13} $b\bar{b}$ will be produced per year – the problem is to trigger on and select the interesting modes. ATLAS and CMS could be competitive for some particular channels, such as $B_d^0 \rightarrow J/\psi K_s^0$ and $B_d^0 \rightarrow \pi^+\pi^-$.

$B^0_d \to J/\psi\, K^0_s$

The decay $B^0_d \to J/\psi\, K^0_s$, with $J/\psi \to \mu^+\mu^-$ and $K^0_s \to \pi^+\pi^-$, is the most appropriate channel to measure the angle β of the unitarity triangle. A way to tag the B^0_d is through the associated B hadron requiring it to decay into lepton + X. The time-integrated asymmetry A is:

$$A = \frac{N^+ - N^-}{N^+ + N^-} = D \cdot \frac{x_d}{1+x_d^2} \cdot \sin 2\beta,$$

where N^+ and N^- are the number of events with positively and negatively charged tagging leptons, D is the tagging dilution factor and $x_d/(1+x_d^2)$ is the time-integration factor. Detailed simulations of these final states have been performed. In CMS a two-muon trigger would be used. The main selection criteria are : i) two muons and ii) two charged hadrons with $p_t > 0.7$ GeV in $|\eta| < 2.4$ for K^0_s reconstruction. Figure 22a shows the $\mu^+\mu^-\pi^+\pi^-$ invariant mass after all selection cuts. To simulate the regime at $10^{33}\,cm^{-2}s^{-1}$, two minimum-bias events have been superimposed on signal and background events. The number of reconstructed signal events is 5500 for $p_t^{\mu\,tag} > 5$ GeV and $10^4 pb^{-1}$. The measured asymmetry A is affected by dilution effects, the most important being mistagging of muons due to oscillations and cascade decays of b ($b \to c \to \mu$) [45]. The overall dilution factor in this channel is D = 0.49 for $p_t^{\mu\,tag} > 5$ GeV and the sensitivity to sin2β ie the expected measurement precision is: $\delta(\sin 2\beta) = 0.05 \pm 0.014$. A time dependent analysis is of similar sensitivity. The sensitivity can be improved using electrons for tagging and in J/ψ decays as done by ATLAS, and is investigated at present in CMS.

$B^0_d \to \pi^+\pi^-$

$B^0_d \to \pi^+\pi^-$ is a promising channel to measure the angle α of the unitarity triangle. Even without particle identification CMS can be expected to perform well thanks to its excellent mass resolution. A trigger is provided by the semileptonic decay of the associated b-hadron which is used to tag the flavour. The main selection criteria are: i) a muon with $p_t^{\mu} > 9$ GeV, ii) two opposite-sign hadrons with $p_t^h > 5$ GeV within $|\eta| < 2$, iii) B^0_d isolation, I < 0.3 ($I = \Sigma\, p_t$ of hadrons within $\Delta R < 1$ around the B^0_d / $p_t(B^0_d)$) and iv) impact parameter significance > 3 for each pion. Without particle identification the two-body decays of B-hadrons generate fake mass peaks when the charged hadrons are assigned a pion mass as visible in Fig. 22b. The background to signal ratio, B/(S + B), is 45% in a mass window of $\pm 1\sigma$ (σ_B = 27 MeV). The combinatorial background gives a flat ~10% background contribution. The number of $B^0_d \to \pi^+\pi^-$ events within a $\pm 1\,\sigma$ mass-bin around the nominal B^0_d peak after all cuts is 4300 [3,45]. Including dilution effects due to oscillations, mistagging and background, the sensitivity to the unitarity triangle angle α is estimated to be: $\delta(\sin 2\alpha) = 0.057^{+0.018}_{-0.014}$. A significant improvement in sensitivity can be obtained using electrons to trigger and tag, but triggering at an electron threshold of E_t ~10 GeV at $10^{33}\,cm^{-2}s^{-1}$ is still under investigation.

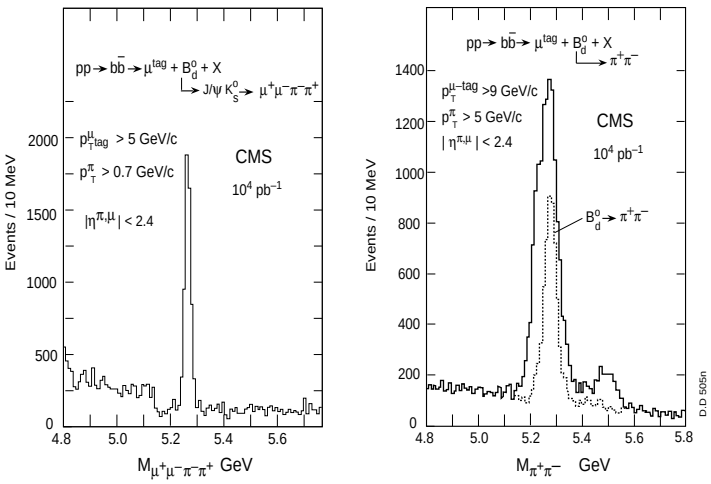

Figs. 22a, b: $\mu^+\mu^-\pi^+\pi^-$ and $\pi^+\pi^-$ invariant masses after all selection cuts.

Perspectives on CP violation measurements

Figure 23 shows the expected sensitivities in the measurements of the unitarity triangle angles α and β in the various experiments over the coming years. A reasonable guess is made for the start-up of the machines and detectors or upgrades as indicated [46, 47, 8, 48]. A data taking and analysis period of at least one year is assumed preceeding the first quoted sensitivity point. For CMS and ATLAS $10^4 pb^{-1}$ is assumed for the first point. Subsequent improvement is due to increased statistics ($1/\sqrt{N}$ behaviour) or to significant detector upgrades as in case of CDF [48]. For each of the experiments there are difficulties. HERA-B is very difficult due to smallness of the B cross section and unfavorable S/B, thus pattern recognition and radiation damage difficulties; for B-factories the machine is critical , if luminosities in excess of $10^{33} cm^{-2} s^{-1}$ are not obtained the statistics will be insufficient for significant results; for CDF and D0 the uncertainties are with the performance upgrades, ultimately they should have comparable reach as ATLAS or CMS as collider experiments are limited by tagging efficiency / purity; LHCB could be the best, but whilst CDF shows that central collider B-physics is feasible, not much can be said up to now on forward B experiments. In any case, around AD 2000 the competition for the first observation of CP violation in the B system may be fierce. The present theoretical lower bound is $\sin 2\beta > 0.17$ [49]. LHC experiments will be the natural higher-sensitivity continuation of these studies.

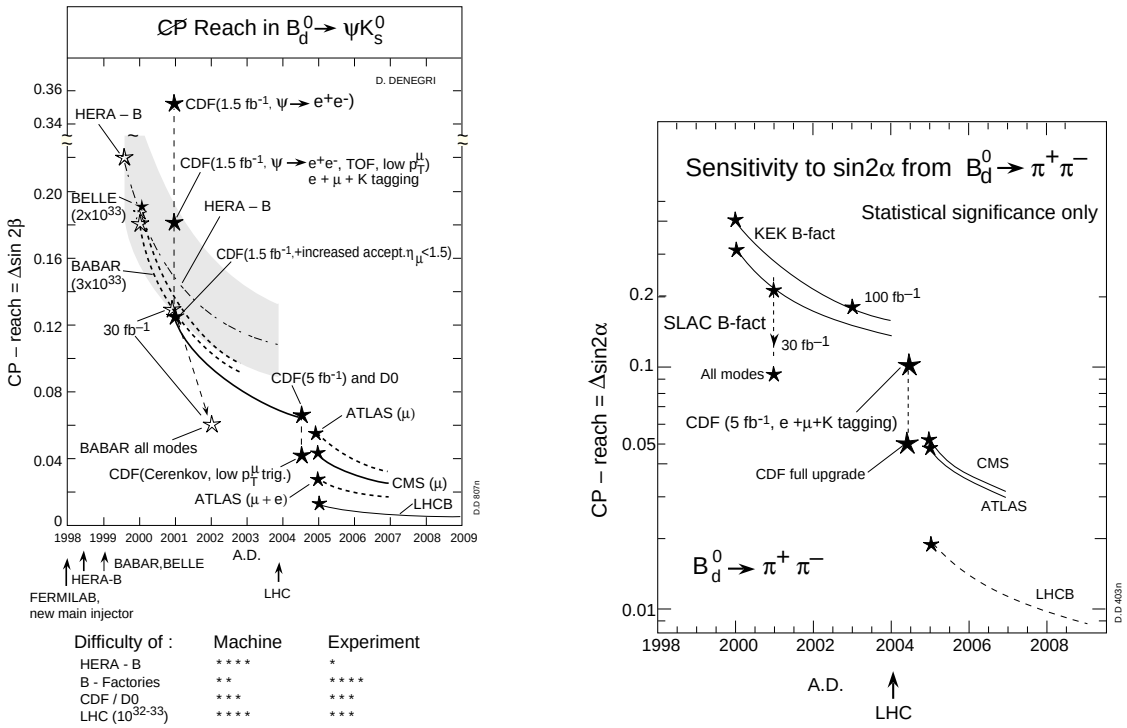

Fig. 23: Expected sensitivities to the measurement of the angles α and β for various experiments over the coming years. The shaded area illustrates the effect of the uncertainty on the B cross section at HERA.

Search for $B_s^0 \to \mu\mu$

$B_s^0 \to \mu^+\mu^-$ is a prototype of a rare decay for which only a hadron collider has a sufficient $b\bar{b}$ production rate to possibly allow its study. The expected SM branching ratio is $\approx 4 \times 10^{-9}$ [50]. The two-muon trigger should be used for $B_s^0 \to \mu\mu$. The background is due to muons from $b\bar{b}$ and a reduction factor of at least 10^7 is needed to suppress it. Appropriate selection criteria are: i) transverse momentum $p_t^{\mu\mu} > 12$ GeV, ii) $\mu^+\mu^-$ pair isolation, iii) a dimuon mass cut, iv) a fight-path cut $d > 3\sigma_{sv}$ and v) $\delta < 0.04$ rad where δ is the angle between the vectors $\vec{p}_t^{\mu\mu}$ and flight-path $\vec{d}$ [45,51]. Critical cuts are the secondary vertex one and the dimuon isolation. In CMS the secondary vertex resolution in the transverse plane is $\sigma_{sv} \approx 70\ \mu m$. After all cuts, 11 signal and less

than 64 background events (at 90% C.L.) are expected for $10^4 pb^{-1}$. The upper limit on the branching ratio which can be set at a 90% C.L. for $10^4\ pb^{-1}$ is 4.5×10^{-9}.

3.4 Heavy ion collisions

Preliminary studies of $Y(Y',Y'') \rightarrow \mu^+\mu^-$ detection in CMS were performed with ^{16}O, ^{40}Ca, ^{97}Nb and ^{208}Pb ion beam collisions. The trigger is provided by the two muons penetrating to the first two muon stations with an effective threshold of $p_t^{\mu} \approx 4$ GeV. The critical aspect is one of pattern recognition for the muons in the midst of the many soft particles [52]. For central Pb–Pb collisions expectations for particle densities go from $dn^{\pm}/dy = 3000$ to as high as $dn^{\pm}/dy = 8000$. Using this latter value in the calculation of occupancy and track reconstruction efficiency in the tracker, the occupancy in the outer four MSGC layers is ~10% (with 25cm long strips) which is at the limit of the acceptable. The muon track reconstruction efficiency in this case is 75% [52].

The cross-sections for *Y* production in A-A collisions are obtained multiplying the cross-sections for pp reactions at the same c.m.s. energy by a factor $A^{2\alpha}$, with $\alpha = 0.95$. The pp cross-section at LHC energies was estimated by extrapolating existing experimental data assuming a linear increase with $\sqrt{s}$, giving $B(d\sigma/dy)_0 = 1.5\times10^{-33}\ cm^2$ at $\sqrt{s_{pp}} \approx 6$ TeV. The earlier estimates were based on the saturating cross section indicated CR in Fig. 23 showing also the recent extrapolations with MRSD structure functions. These would give a factor~2 larger cross section still [53]. The main dimuon background is due to uncorrelated muon pairs from π,K decays, the contributions from b and c decays are less significant [3].

Dimuon mass spectra expected from a typical experimental run with Pb, Ni and Ca beams assuming the high particle density option in each case and no colour supression are shown in Fig.24. The mass resolution is 85 MeV (FWHM). The signal-to-background ratios indicated for Pb collisions have been calculated in the mass band $M(Y) \pm 50$ MeV. For lighter nuclei the S/B ratio improves, as well as the overall production rate, Fig.24. The plan is to measure the production ratios of *Y*(2S) and *Y*(3S) relative to *Y*(1S) with different ion species, possibly at different energies, and relative to pp collisions, and correlate it with the centrality of the collisions measured by the calorimetric global or transverse energy flows. Colour screening resulting in the suppression of all heavy quark bound states except for *Y*(1S) is the signature of quark-gluon plasma formation that would be investigated [10]. Another probe of QGP formation is jet production, where jet quenching is expected [54]. The CMS 4π calorimetry could allow to test this signature too [55].

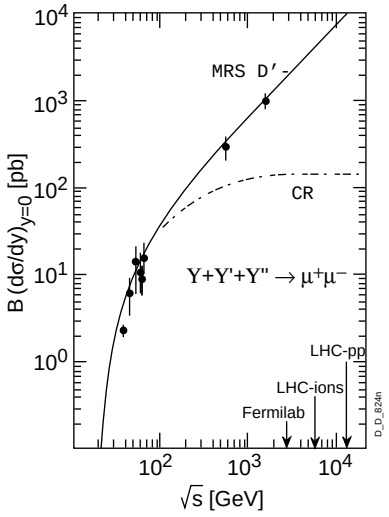

Fig. 23 Energy dependence of Y production in pN

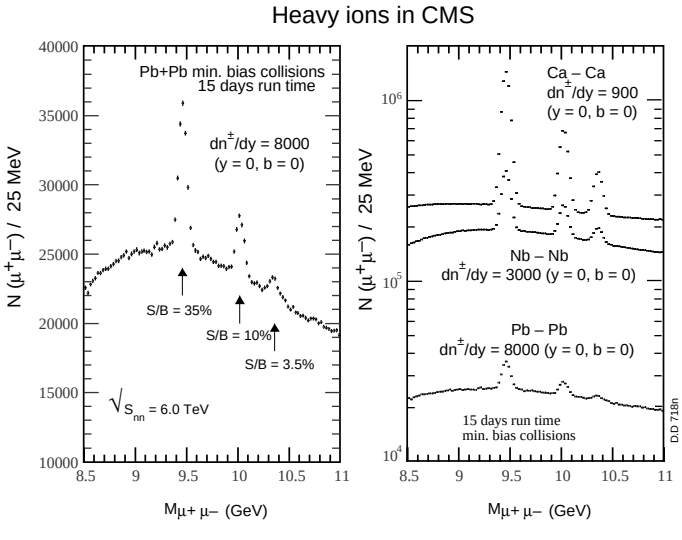

Fig. 24: Mass distributions of opposite sign muon pairs for Pb-Pb, Ni-Ni and Ca-Ca collisions in CMS.

4. CONCLUSIONS

The main task at the LHC will be to shed light on the mechanism responsible for electroweak symmetry breaking. The simplest scenario is the SM Higgs one, the MSSM one is its simplest supersymmetric extention, but no-elementary-Higgs and non-resonant schemes are possible too [2]. CMS and ATLAS are powerful and well balanced general pourpose detectors able to thoroughly explore these possibilities through a variety of experimental signatures. The entire expected SM Higgs mass range can be explored, and with few$\times 10^5 pb^{-1}$ the MSSM definitively tested. Even if ew symmetry breaking is not realised through a Higgs mechanism, the detector designs are flexible enough that they would allow to explore a number of alternative symmetry breaking schemes [1,2]. A hadron collider is also the most appropriate machine to look for squarks and gluinos; the LHC will allow to cover the mass range where supersymmetry could be of relevance for ew symmetry breaking. The lightest supersymmetric particle, if a neutralino, is of key cosmological importance being a prime candidate for dark matter. A mass range up to ~0.2 TeV can be explored indirectly through squark, gluino, chargino, neutralino or slepton searches. Very exciting possibilities exist too for CP violation studies in the B system and for uncovering and studying QCD deconfinement.

5. REFERENCES

[1] G. Altarelli, Proc. of LHC Workshop, Aachen, CERN 90-10, 1990 and references therein;
M. Lindner, Z. Phys C31 (1986) 295;
M. Chanowitz, Ann. Rev. Nucl. Part. Sci. 38 (1988) 323.

[2] S. Dimopoulos and M. Lindner, Proc. of LHC Workshop, Aachen, CERN 90-10, 1990.

[3] Technical Proposal, CMS Collaboration, CERN / LHCC 94-38, LHCC / P1, December 1994;
Letter of Intent, CMS Collaboration, CERN / LHCC 92-3.

[4] Technical Proposal, ATLAS Collaboration, CERN / LHCC / 94-43,LHCC / P2, December 1994.

[5] H. Baer et al. Low Energy Supersymmetry Phenomenology, CERN-PPE / 95-45, April 1995;
H. Baer et al., Phys. Rev. D50 (1994) 4508;
R. Barbieri et al. , NP B367 (1993) 28.

[6] Z. Kunszt and F. Zwirner, Nucl. Phys. B385 (1992) 3.

[7] P. Sphicas, CDF Collaboration, "Four Seas Conference", Trieste, June 1995 and Proc. SLAC Summer Institute 1995, July 1995;
J.A. Mueller, 'Beauty 94', M. St. Michel, France, May 1994, NIM A 351 (1994) 59.

[8] Letter of Intent, LHC-B Collaboration, CERN / LHCC 95-5, LHCC / I8, August 1995.

[9] Letter of Intent, ALICE Collaboration, CERN / LHCC93-16, March 1993.

[10] T. Matsui and H. Satz, Phys. Lett. B178 (1986) 416.

[11] F. Gasparini et al., Nucl. Instrum. Methods A336 (1993) 91.

[12] R. Cardarelli et al., Nucl. Instrum. Methods A340 (1994) 466;

[13] D. Carlsmith, CMS Cathode Strip Chambers in Endcap Magnetic Field, CMS TN / 94-217 (1994);
Y. Fisyak and J. Rowe, CMS TN / 94-160 (1994).

[14] F. Angelini et al., Nucl. Instrum. Methods A343 (1994) 441;

[15] V. Karimaki, Fast tracker response simulation, CMS TN / 94-275 and references therein;
A. Khanov and N. Stepanov, Fast track finder algorithm, CMS TN / 94-309;

[16] D.J. Graham, An algorithm using tracks to locate the two-photon vertex at high luminosity, CMS TN / 95-115.

[17] C. Seez and T.S. Virdee, The Higgs to two photon Decay in CMS, an update, CMS TN / 94-289 and references therein.

[18] P. Lecoq et al., Lead tungstate scintillators for LHC em calorimetry, CMS TN / 94-308 (1994);

[19] E. Lorenz et al., Max Planck Institute, Munich, MPI-PHE-93-23 (1993);

[20] PbWO4 test beam results, CMS working group meetings 1995;
J.P. Peigneux et al. , Results from tests on matrices of lead tungstate crystals using high energy beams, CMS TN / 95-166.

[21] A. Nikitenko, P. Verrecchia and D. Bomestar, GEANT reconstruction of $H \rightarrow ZZ^* \rightarrow 4e$, CMS TN / 95-019 (1995);

[22] A. Ferrando et al., CMS TN / 92-19 (1992);
[23] O. Ganel and R. Wigmans, SSC note SDC-93 / 575 (1993);
[24] F. Abe et al., CDF collaboration, Phys. Rev. Lett. 74 (1995) 2676.
S. Abachi et al., D0 Collaboration, Phys. Rev. Lett. 74 (1995) 2632.
[25] J. Ellis, G.L. Fogli and E. Lisi, The Higgs Boson Mass from Precision Electroweak Data, CERN TH / 95-202 (1995) and CERN–TH 7261 / 94; J. Ellis, New fits to m_{Higgs}, communication at the CMS Physics Meeting, October 1995.
[26] LEP Electroweak Working Group, CERN Report no. LEPEWWG / 95-01,
[27] J.F. Grivaz, "New Particle Searches", LAL 95-83, rapporteur talk at EPS Brussels Conferece, July 1995;
F. Richard, contribution to International Conf. on High Energy Physics, 94- Glasgow.
[28] M. Lindner, Z. Phys C31 (1986) 295; M. Sher, Phys. Rep179 (1989) 273;
G. Altarelli, Proc. of LHC Workshop, Aachen, eds G. Jarlskog and D. Rein, CERN 90-10, 1990;
see also R. Barbieri, talk at this conference and ref.[22].
[29] K. Lassila, $H \to \gamma\gamma$ conversion recovery, mass resolution, communications in CMS working groups.
[30] S. Abdullin et al. , 'Possibilities to improve the observability of SM light Higgs in the $\gamma\gamma$ channel', CMS TN / 94–247 (1994).
[31] I. Iashvili et al., 'Study of $H \to ZZ^* \to 4l^{\pm}$ inCMS', CMS / TN 95-059.
[32] D. Bomestar et al., Study of $H \to ZZ \to 4l^{\pm}$ with full GEANT simulation of CMS, CMS TN / 95-018.
[33] M. Dzelalija et al., 'Study of Heavy $H \to ZZ \to 4l^{\pm}$ inCMS, 'CMS TN / 95-076.
[34] S. Abdullin and N. Stepanov, CMS TN / 94–179 (1994) and CMS TN / 94–178 (1994).
[35] G. Kane et al., 'Study of Constrained Minimal Supersymmetry', UM- TH-93–24 (1993);
J.A. Casas et al., ' The Lightest Higgs Bosons Mass in the Minimal Supersymmetric Standard Model', CERN–TH.7334 / 94 (1994).
[36] We are highly indebted to Z. Kunszt and F. Zwirner, who provided us with their programs RADCORR and BBSUSY.
[37] R. Kinnunen, J. Tuominiemi, D, Denegri, CMS TN / 93–98 (1993) and TN / 93–103 (1993).
[38] R. Kinnunen et al., CMS TN / 94–233 (1994).
[39] D. Denegri, et al., 'Justifications for a pixel detector in CMS', CMS TN / 94–258.
[40] N. Stepanov, CMS TN / 94–182 (1994);
C. Kao and N. Stepanov, Discovering MMSM Higgs Bosons with Muons,UR-1407,ER-40685-854,1995.
[41] J. Dai, J. F. Gunion and R. Vega, UCD-93–20, SLAC PUB-6277.
[42] J. M. Benlloch, CDF Collaboration, XXX th Rencontre de Moriond, QCD and High Energy Hadronic Interactions, March 1995; D. Claes, presentation at the 10th Topical Workshop on Collider Physics, FERMILAB, May 1995.
[43] V. Genchev and M. Greiter, Backgrounds for the SUSY Searches, CMS TN / 95-066;
V. Genchev, Gluino and squark searches at LHC, "Four Seas Conference", Trieste, June 1995.
[44] L. Rurua, CMS TN / 94–207 (1994).
[45] D. Denegri et al., Int. Journal of Mod. Phys A,Vol 9, No 24 (1994) 4211; D. Denegri, et al., in 'Beauty 94', M. St. Michel, France, May 1994, NIM A 351 (1994) 95.
[46] HERA-B Proposal, DESY-PRC 94 / 02, May 1994; P. Krizan et al., in 'Beauty 94', NIM A 351 (1994) 111.
[47] G. Wormser, 'Beauty 94', M. St. Michel, France, May 1994, NIM A 351 (1994) 54; G. Wormser LAL preprint 95-85; BABAR Technical Design Report, SLAC-R-95-457, March 1995.
[48] N.S. Lockyer, B physics at CDF and D0, Present and Future, CDF / DOC / BOTTOM / PUBLIC / 3039;
F. DeJongh, B physics with CDF RunII upgrade, "Four Seas Conference", Trieste, June 1995.
[49] A. Ali and D. Landon, CERN–TH 7398 / 94.
[50] B. Buchalla and A. Buras, Nucl Phys. B400 (1993) 225;
A. Ali, C. Greub and T. Mannel, 'Rare B Decays in Standard Model', DESY 93–016 (1993).
[51] A. Nikitenko and A. Starodumov, CMS TN / 94–186.
[52] O. Kodolova and M. Bedjidian, Pattern recognition and track reconstruction in heavy ion collisions, CMS TN / 95-124.
[53] R. Gavai et al. Int. Journal of Mod. Phys. A,Vol 10 (1995) 3043.
[54] H. Satz, ECFA LHC Workshop Proceedings, CERN 90–10,
[55] R. Kvatadze and R. Shanidze, CERN CMS TN / 94–270 and V. Korotkikh, et al., CERN CMS TN / 94–244.